THE HIGH TEMPERATURE EROSION OF THERMALLY SPRAYED METALLIC COATINGS BY SOLID PARTICLES

By

P.J. HOOP

A thesis submitted to the Faculty of Engineering,
University of Cape Town, in fulfilment of the Degree of
Master of Applied Science

August 1998

Department of Materials Engineering

Abstract

Erosion testing has been carried out on a series of commercial thermally sprayed, hard coatings applied to boiler tubes in the power generation industry. Testing was performed at 400°C in a specially designed high temperature erosion rig (HTER), which is capable of simulating conditions encountered in boiler plants using silica sand (SiO_2) as the erodent.

Erosion rates have been determined through mass loss measurements for eight coatings at a constant erodent velocity of 24 $m.s^{-1}$, a mass flux of 0.21 $kg.m^{-2}.s^{-1}$ and an impact angle of 40°. The erosion rate of the different coatings has been compared to the erosion rate of the boiler steel, which was used as the standard reference material.

It was found that only four of the coatings, which had predominantly tungsten carbide (WC) in their microstructure, exhibited a lower erosion rate than the boiler steel. Whilst the erosion rates were found to increase with decreasing coating hardness, it has been shown that hardness alone is not a good guide to erosion resistance. Explanations for the large differences in erosion behaviour have been advanced based on the influence of the microstructure coupled to the mechanism of material removal.

Scanning electron microscopy revealed typical features associated with a ductile erosive wear process for the boiler steel. Extensive surface deformation and ploughing and the appearance of craters and lips were observed. Single solid particle impacts on a polished coating surface showed that chipping occurred at phase and oxide interfaces. This mechanism of material removal was found to be very different than simple ductile erosion and lead to higher erosion rates.

A strong correlation has been established between increasing erosion rate and increasing porosity in the coatings. It was found that in general coatings with a fine microstructure, in which defects were small and well dispersed, had the best erosion resistance.

TABLE OF CONTENTS

List of Figures

List of Tables

Chapter 1

Introduction

High temperature erosion is a serious problem in coal fired power stations in South Africa because of the interaction of ash particles with boiler tubes. This can lead to costly outages and production losses. For example, a total of 23 fly ash related boiler tube failures were reported in 1996 resulting in a total load loss of some 610 000 MW hours in the power generating industry in South Africa.

Efforts to control the fly ash erosion problem have included the use of perforated screens in strategic areas of the boiler to even out hot gas flow distribution and to reduce peak velocities of the ash together with washing of the coal to reduce the quantity of hard minerals. Recently, thermally sprayed metallic coatings have been increasingly applied to boiler tubes in an attempt to lower the erosion rates and thus increase the boiler tube life. The concept of coating surfaces to give protection against environmental attack is long established and has found application in many forms and across a wide variety of disciplines. Despite the great variety of coating types and their utilisation, the basic requirements for surface protection are generally valid for all systems: good environmental resistance, long term stability of the protective layer and strong adhesion to the substrate [1].

Several coatings are being employed in power plants, which have different chemical compositions and properties. This implies that the erosion resistance will vary from coating to coating. The coatings are mixtures of more erosion resistant alloys and are specially formulated to have good high temperature properties and excellent erosion resistance. The metals most widely used for this purpose are chromium (Cr), molybdenum (Mo) and nickel (Ni).

Whilst it has been reported that a uniformly deposited and coherent metallic coatings can provide erosion protection, no systematic experimentation has been undertaken to qualify the

erosion performance of these materials. This work is an attempt to examine the erosion behaviour of a series of commercial thermally sprayed coatings at a temperature of 400°C, where boiler tubes are found to be most vulnerable to erosion damage.

The objectives of this work were three-fold

1) to rank a series of thermally sprayed coatings used in South African boiler plants in terms of their erosion resistance at 400°C.

2) to determine the effect of material constitution and properties on the erosion rate of eight coatings.

3) to relate the wear mechanisms and erosion rates for the coatings and the boiler steel.

Chapter 2

Literature Review

2.1. The Process of Erosion

When solid or liquid particles continuously strike a surface, parent material will be gradually removed. This process is known as erosion [2, 3]. Tabakoff et al [4] defined the rate of erosion as the ratio between the sample mass loss and the mass of the impacting erodent particles, i.e.

Erosion rate = (change in sample mass)/(mass of erodent particles)

The extent of erosive wear is dependent on a number of factors. These include the number and mass of individual particles striking the surface, impact velocity, temperature, impact angle, morphology and type of erodent, mass flux and the effect of erosion-corrosion. These variables are fully discussed in Section 2.2. The erosion rate is further dependent on a number of material properties, such as hardness, surface profile, microstructure, coating-substrate adhesion and porosity. These properties are discussed at length in Section 2.4.

Two types of erosive wear processes have been identified by Benchaita et al [5]. These are ductile wear and brittle wear.

2.1.1. Ductile wear

Hutchings [2] considered three basic types of impact damage on a ductile material:

a) Ploughing

During this process material is displaced to the side and in front of rounded particles. Further impacts lead to the removal of heavily strained material from the crater that had formed as shown in Figure 2.1(a).

b) Type I cutting

This type of deformation is caused by angular particles and depends on the orientation of the particle when it strikes the surface. The particle rolls forward during impact, indenting the surface leading to the formation of lips which are removed by subsequent nearby impacts as illustrated in Figure 2.1(b).

c) Type II cutting

This type of deformation is caused by angular particles rolling backwards, during which a true machining action occurs. The sharp corner of the abrasive grain cuts a chip from the surface as shown in Figure 2.1(c).

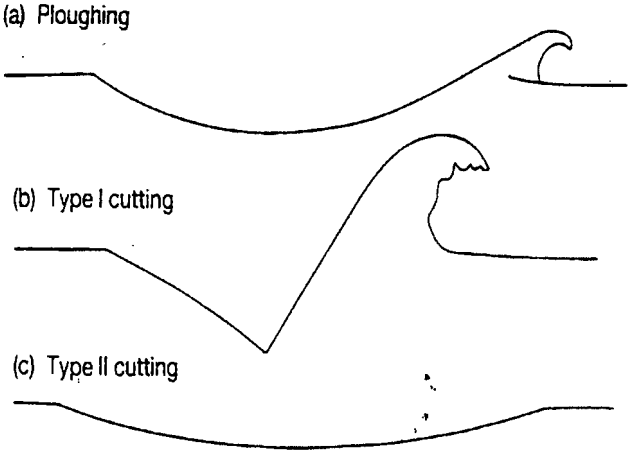

***Figure 2.1:** Three different wear mechanisms on a ductile material [2].*

Sundararajan [6] showed that the angle at which maximum wear takes place for spherical particles to be 40° for ductile materials. Further, Suckling and Allen [7] showed that for a 106-125 μm plant fly ash, the angle at which maximum wear takes place is between 30 and 40°.

By investigating the eroded surfaces of specimens tested at 30° and 90°, Levy et al [8] found that the mechanism of material removal for ductile metals does not change with impact angle. In single-phase ductile materials the basic erosion mechanism is considered to be a combination of micromachining and ploughing processes and damage accumulating processes [9]. Levy et al [10] found that after many impacts the surface becomes covered with

displaced deformed material, which forms "platelets". The platelet displays ductile cracks around the edges and can be removed by subsequent particle impacts. Evidence was found that related higher erosion resistance to high ductility rather than to hardness or strength [11, 12].

For their part, Bellman and Levy [13] proposed that the plastic deformation caused by erosive particles leads to a temperature rise in the near-surface material which is high enough to stress relieve or anneal the material. Shewmon [14] and Hutchings [12] related the heating effects due to deformation of impacting particles to the particle size. The assumption of either adiabatic or isothermal heating was examined by Doyle and Ball [15]. They compared the ratio of the depth of the plastic zone, which is associated with impact deformation, to the root mean square diffusion distance of heat from the impact site. This approach enabled them to see the nature of the thermal conditions at the impact sites. It was found that the ratios for 100°C and 600°C were 1.2 and 1.5 respectively. For ratios $>> 1$, conditions can be assumed to be adiabatic and $<< 1$, conditions are isothermal. It is clear that the case is neither strongly for the assumption of adiabatic conditions nor against. It was concluded that thermal effects during solid particle erosive wear for the specific conditions can be ignored.

Several researchers have studied the microstructure around single particle impact sites on ductile materials and found dense dislocation entanglements close to the indentations [16, 17, 18]. However Brown et al [19] found evidence of recrystallisation in erosion debris recovered from eroded specimens. They suggested that recrystallisation occurs by a combination of a temperature rise and the very high strain rate associated with surface deformation. Cousins and Hutchings [20] found that the erosion rate with spherical particles on ductile materials is lower than that due to angular particles with the same size.

2.1.2. Brittle wear

Various researchers have found that the angle at which maximum material loss occurs to be 90° for brittle materials [4, 21]. Hutchings [2] states that impacting particles cause brittle fracture when material is removed from the surface through the formation and intersection of cracks. He found that some plastic flow occurred around the point of contact for angular particles. In single-phase brittle materials a single erosion mechanism is thought to be

operative. This mechanism involves the generation and propagation of subsurface lateral cracks driven by the residual stresses produced in an elastic-plastic contact zone [22].

Scattergood and Routbort [23] suggested significant temperature rises in brittle materials, which deform only locally, directly under the impacting particles. Wada and co-workers [24, 25] have shown that the properties of erodent particles affect the erosion rate and crack morphology of brittle materials. They reported an increase in the erosion rates when the ratio of the hardness of the particle, H_p, to the hardness of the target material, H_t, was increased. The erosion rates increased markedly at the transition point $H_p/H_t = 1$. It was reported that the accepted mechanistic model for erosion in brittle materials involved the propagation of lateral cracks [26, 27]. The elastic-plastic impacts of sharp particles produce a damage zone where residual tensile forces generate and propagate sub-surface lateral cracks [28]. The erosion rate is given by

$$\Delta E \propto c^2 \times h$$

where, ΔE = change in erosion rate, c = lateral crack extension, h = depth of lateral cracks. From standard fracture mechanics [29], the equilibrium crack extension was established to be

$$c = 1/\Pi \times (P/K_{IC})^{2/3}$$

where, c = equilibrium crack extension, P = load, K_{IC} = toughness.

Ceramics have been found to be susceptible to surface cracking when impacted by sharp, hard particles. The impact damage can be modelled by the idealised flaw system produced by a sharp indentor such as the Vickers diamond pyramid [30, 31, 32]. The indentor produces two distinctive crack systems: radial cracks, leading to strength degradation and lateral cracks, leading to material removal.

2.2. Factors Affecting the Erosion Rate

As previously mentioned there are many factors that affect the erosion rate. These factors are considered in this section.

2.2.1. Temperature

Smeltzer et al [33] discussed the question of the effect of temperature on erosive wear and is in agreement with Raask [34] who states that with increasing temperature there is an increase in erosion rate until a critical temperature is reached where erosion rate decreases. This is due to the competition that exists between oxide layer formation and material removal by erodent particles.

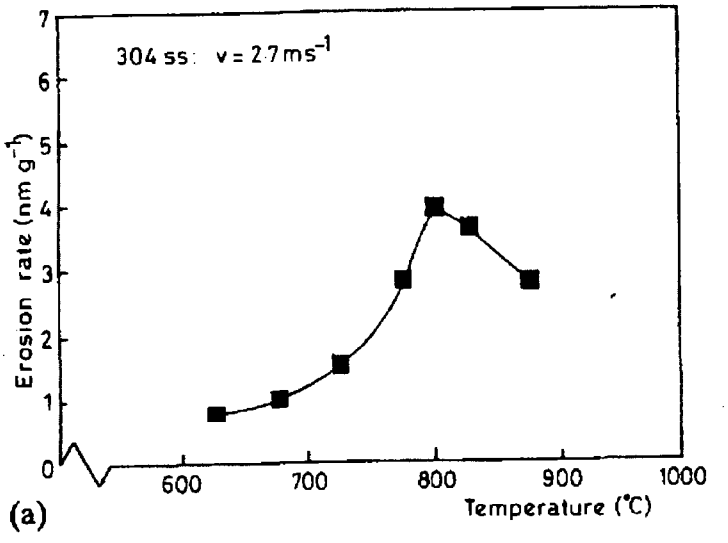

Figure 2.2: *Variation of erosion-corrosion with temperature in low velocity erosion-corrosion systems [14].*

The peak in the wastage Vs temperature curve moves to higher temperatures and wear rates with increasing particle impact velocity [35, 36]. The curve also shifts to higher temperatures when the alloy oxidation resistance increases [37, 38, 36]. It is believed that erosion is the dominant process at low temperatures but the formation of oxide increases exponentially as the temperature increases which becomes dominant at high temperatures [21], i.e.

$$K_p = K_0 \times e^{-KT}$$

K_p = parabolic rate constant

K_0, K = constants

T = temperature

From room temperature testing it was discovered that the surface region undergoing erosion is heated to relatively high temperatures by the severe plastic deformation that occurs [39, 40].

2.2.2. Erosion-Corrosion

Dils and Follansbee [41] suggested that material loss can occur without the interaction of erodent particles because of cyclic thermal and hence mechanical strains experienced by the oxide layer. The oxide layer cracks during thermal cycling, leading to spalling. A similar view is held by Cathcart and Pawel [42]. There is a generally held view amongst researchers investigating erosive wear in fluidised bed boiler situations that there is a peak in material wastage in ferritic alloys which varies as a function of particle velocity, size, shape and the corrosion resistance of the target material [43, 21, 44, 45]. Stack et al [21] based their understanding of peak phenomena on a transition from erosion dominated to corrosion dominated behaviour.

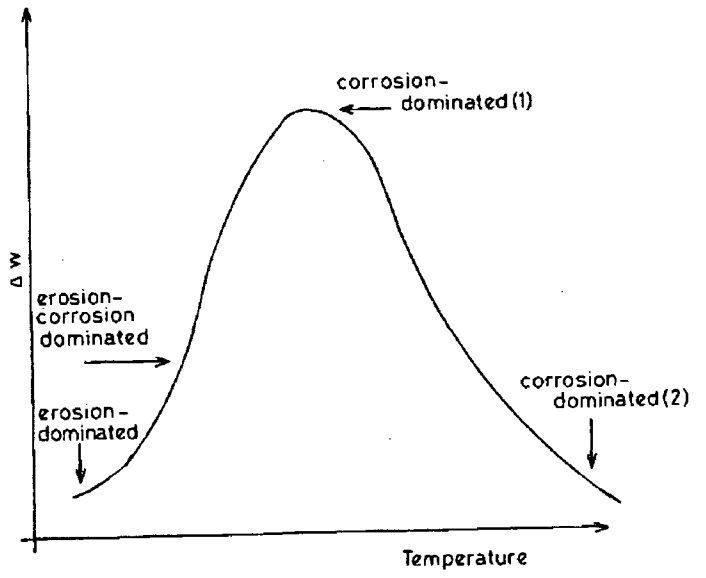

***Figure 2.3:** Diagram showing the variation of the weight change with temperature in erosion-corrosion environments [14].*

Wang et al [45] eroded a 1018 steel and found that material wastage decreased upon formation of an adherent oxide layer. A model has been proposed regarding the removal of corrosion products from the parent material [46, 47]. It was discovered that chromia and alumina scales formed in situ on chromium containing or aluminium containing alloys respectively. The scales behaved in a brittle manner like other ceramic materials. The 2.5 μm thick scales lost material in sequentially removed layers by a mechanism of cracking and chipping.

Nicolls [48] suggested that in some instances, corrosion and erosion might be present together. The time at which the transition from the initiation stage to the propagation stage takes place is reduced when erosive conditions are present along with the conditions causing hot corrosion attack. It is believed that the erosion causes hot corrosion to be more severe by reducing the thickness of the porous scale formed on the surfaces of alloys and coatings. Other investigations that combined erosion and corrosion determined that, under most test conditions, corrosion is the dominant mechanism and that the erosion of corrosion scale products and not the erosion of the substrate metal is occurring in combined testing [49, 50, 51].

The particle kinetic energies required to cause material loss are likely to be lower under erosion-corrosion conditions than under erosion alone. The erosion-corrosion rates as a function of temperature show that there exists a transition temperature below which the erosion-corrosion rates are relatively insensitive to the temperature [52]. At high temperatures the rates increase sharply. Nicolls [48] further suggested that the erosion-corrosion rate of a 2.25 Cr - 1 Mo steel at high temperatures depended on the erodent feed rate while the rates for type 304 stainless steel are independent of the feed rate. The results are described for a mechanism that involves fracturing, chipping and other damage to the oxide and the oxidation kinetics.

2.2.3. Erodent flux

Wright, Sethi and Nagarajan [53] found that the rate of erosion-corrosion can be determined by the erodent flux, since the time available for oxide growth (or re-growth) in a given area is determined by the interval between successive erodent impacts. Wood [54] found that the flux of materials affected their interaction with the surface being eroded. At high fluxes, it appears that particles pile up at the specimen surface and collisions between impinging and recoiling particles become more significant (Figure 2.4). The "traffic" at the surface becomes too heavy and the erosion rate falls.

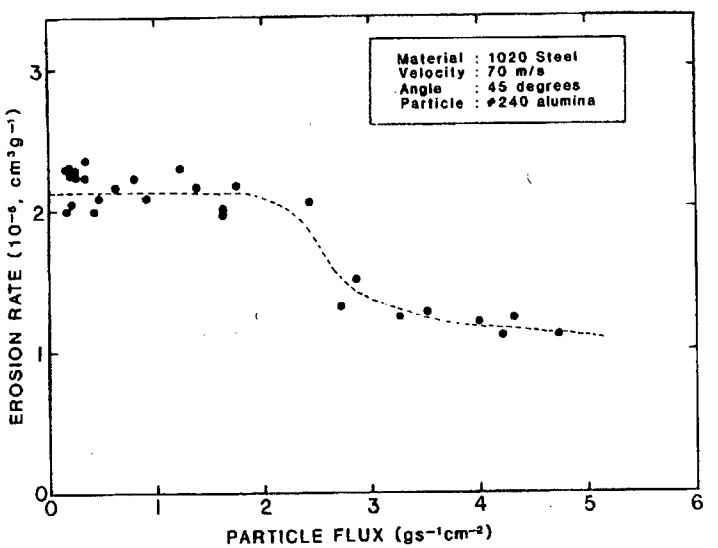

***Figure 2.4:** The graph shows that the erosion rate decreases at a surface because of particle congestion when the flux is high [54].*

2.2.4. Impact angle

Tabakoff et al [4] found that for ductile materials the erosion rate increased to a maximum as the impact angle is increased. After reaching a maximum, the erosion rate decreased to a minimum value at 90°. They found that the erosion rate of brittle materials increased to a maximum value at 90°. The impact angle is generally used to assign whether the erosion process is "ductile" or "brittle" [21]. When the erosion rate peaks between 15° and 30° the process is "ductile", but when the erosion rate is at a maximum at 90°, it is classified as "brittle". These results were obtained by Stack et al [21] when they investigated the effect of

impact angle on the erosion rate of ductile aluminium and brittle alumina. Laitone [55] has defined two cases dealing with two phase flow:

1) In the limiting case where all the particles are sufficiently small that the airstream density approaches that of the fluid, the particles do not impact the surface but follow the fluid streamlines around the target.
2) As the particles momentum increases, the trajectory of the particles deviate from the fluid streamlines. In the case where the particles have a high momentum the particles travel in straight line trajectories determined by the initial conditions.

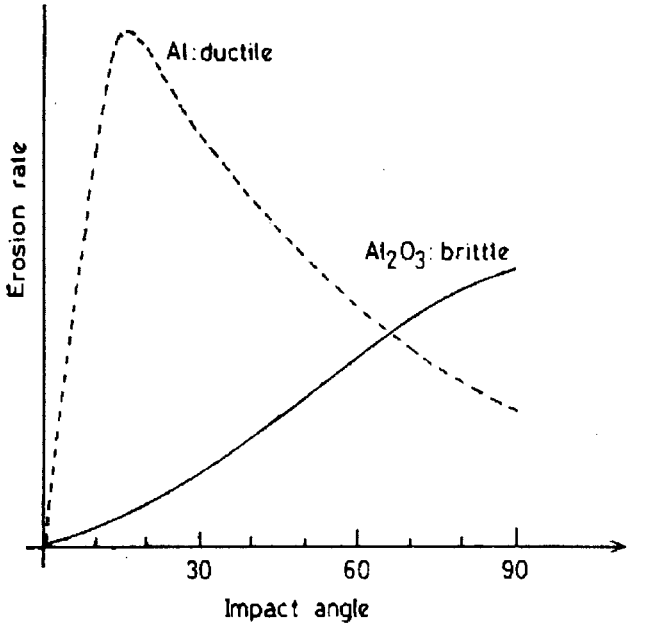

***Figure 2.5:** Schematic diagram showing the erosion rate Vs impact angle for ductile aluminium and brittle alumina [21].*

2.2.5. Velocity

Tabakoff et al [4] investigated the effect of velocity on the erosion rate of a series of coatings and stainless steel in their wind tunnel erosion rig. They found that the erosion rate generally increases with an increase in the impact particle velocity. A power law curve fit was obtained by plotting the erosion rate against the velocity at different angles. The velocity exponent was obtained from the slope of the graph. Different velocity exponents were obtained for the series of coatings and stainless steel. Tabakoff and co-workers [4] concluded that the

different values obtained at the same test conditions were an indication of the material properties effect on the erosion behaviour.

The wastage rate Vs temperature curves shifted to higher rates and temperatures when the velocity was increased [36]. This is because, the time between impacts decreases when the velocity increases and at the same time the energy of the particle increases. It was found that the relationship between the erosion rate and the velocity is given by

$$E = Kv^n f(\theta)$$

where E = erosion rate, K = constant, v = velocity, n = velocity exponent and θ = impact angle

2.2.6. Erodent

Bahadur and Badruddin [56] reported greater erosion rates for both ductile and brittle materials with angular particles. It has been shown that the shape and hardness of the particles determine the depth of the impact in the target material and hence affects the erosion rate of the material [6]. Wada [57] found that increasing the ratio of target hardness to the hardness of the impacting particle (H_t/H_p) results in a dramatic increase in the erosion rates. Erosion rates were determined for ratios in the ranges of unity using particles 1 mm in size.

When erodent particles are slightly harder than the target materials, the erosion rates are relatively high [58]. There is a sudden decrease in erosion rates when the hardness ratio equals unity, whereafter the erosion rates decrease slightly with increasing coating hardness. Vaughan reported that the fracture toughness of a particle determines whether the particle will fragment on impact, hence absorbing some of the impact energy. This reduces the energy that is transferred to the target. This will consequently reduce the erosion rate [59].

2.3. Thermal coatings

2.3.1. Introduction

The various processes of thermal spraying are generally based on methods by which a metallic or non-metallic wire or powder is melted [60] and the fused particles projected on to a prepared surface to build up an adherent coating. Several methods are used to apply coatings to the substrate surface including, plasma spraying, flame spraying, detonation gun technique, low pressure plasma spraying, electric arc spraying, laser-assisted techniques, and the high velocity oxygen fuel technique (HVOF).

Thermal spraying is a very successful and versatile process because of the wide range of coating materials and substrates that can be processed, e.g. tape recording heads, print rollers and even bridge structures [61]. The normal procedure for thermal spraying involves two steps: surface preparation and coating application. The former is a blasting operation to remove all surface oxides and to achieve a clean metallic surface. This process takes about 20 minutes. Coating application must be made four hours after blasting to avoid oxide formation. The total time for coating application is much shorter compared to other protective measures [62]. Bennett and Quigley found that mechanised spraying is preferred for large areas of straight tubing, while manual spraying could be used for curved tubing and for smaller areas [63].

2.3.2. Coating application processes

2.3.2.1. Plasma spraying

In this process a DC electric arc is formed between the nozzle and the electrode. A stream of hot gases is passed through the arc resulting in the dissociation and ionisation of the gases. This produces a high temperature plasma stream from the gun nozzle. Temperatures up to 16000°C can be produced. In practice most coatings will be deposited with a flame temperature in the range 6000°C to 11000°C. The system utilises powder materials for deposition. The powder is suspended in a carrier inert gas (e.g. argon) and is accompanied by

hydrogen (H) to increase the power level. According to Steffens [60] plasma coatings offer the following technical advantages:

- high particle velocity resulting in high bond strength and density
- the heat source is more efficient, thus providing efficient particle heating
- the heat source is inert, minimising oxidation
- higher plasma temperatures permit the spraying of materials with higher melting points

In a low-pressure atmosphere, particle velocity can be significantly increased. In addition, any harmful gas-metal reactions can be avoided. Coatings of high quality and chemical purity may be produced.

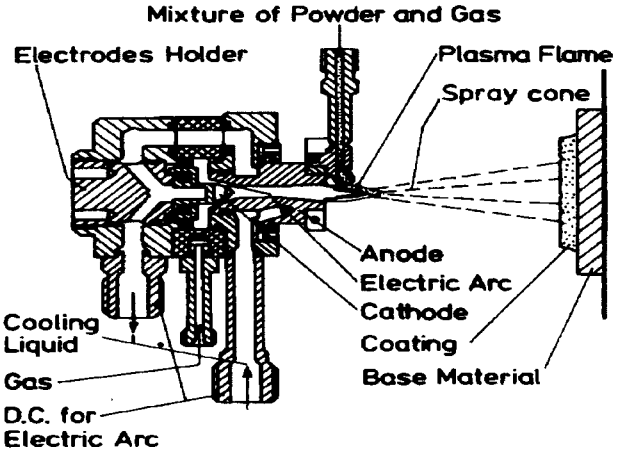

***Figure 2.6:** Illustration of the apparatus used for the plasma spraying technique [60].*

2.3.2.2. Flame spraying

2.3.2.2.(a) Wire Spraying

A wire 3.5 mm in diameter is fed by a variable speed motor of air turbine through the centre of a multi-jet combustion flame. The tip melts and the gas jet strips molten particles from it and propels them to the substrate at a velocity of about 100 $m.s^{-1}$. The gas used is normally acetylene. Wire spraying equipment is portable and can be used manually. Thus, they are used for on-site applications.

2.3.2.2. (b) Powder spraying

In this process the combustion gases are mixed and burnt in a region around a central powder injector. The powder is mixed into the gas stream by a powder feed unit. The particles become partially or fully molten and reach velocities up 100 $m.s^{-1}$ from the flame. Compressed air can be used to further accelerate the particles.

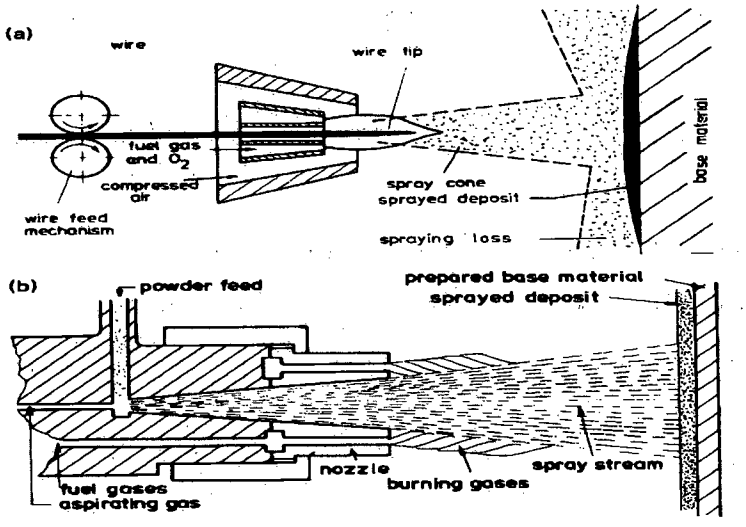

Figure 2.7: *Schematic of the flame spraying technique for coating application [60].*
(a) wire form and (b) powder form

2.3.2.3. The detonation gun technique

The detonation gun consists of a barrel 1 - 1.5 m long and 20 - 30 mm internal diameter in to which the gas mixture is injected and ignited by a spark plug. Upon reaching a critical temperature, self-ignition produces a detonation or shock wave. For equi-molar ratio of oxygen and acetylene this wave travels at about 3000 $m.s^{-1}$ and at a maximum temperature of 3500 K. The particles can be accelerated to velocities exceeding 700 $m.s^{-1}$, producing good bonded and high density thermally sprayed coatings. This technique yields a circular area of about 250 mm^2 and 6 μm thick.

However the erosion rate of mild steel decreased with increasing impact angle, while the ceramic erosion rate still increased. For mild steel maximum erosion occurred at an angle of 30° (ductile materials).

For brittle materials maximum erosion occurred at normal impact angles. In the second series of tests, mild steel, an alumina ceramic and a range of thermally applied coatings were tested at a temperature of 650°C using 180 μm quartz particles (coatings were also tested at ambient temperatures). Again it was found that the erosion rate increased with particle velocity and particle size for both mild steel and the alumina ceramic. The same conditions applied for erosion rate versus angle of impingement (see above). It was also discovered that the erosion rate increased rapidly with increasing temperature.

2.4. The Effect of Coating Variables on the Erosion Rates

2.4.1. Porosity

Coatings with a high erosion rate exhibited a high degree of porosity [64]. Porosity can be assessed from metallographic sections and the introduction of quantitative metallographic techniques can greatly facilitate this. Alternatively, a measure of interconnected porosity can be derived from the oil immersion technique, while an overall density value can be obtained on a piece of coating removed from the substrate. The presence of porosity lowers the hardness compared with that of the bulk material [65]. Vladimir [66] found that porous regions form because of the following reasons:

a) An incomplete coverage of surfaces on the incidence of droplets
b) An interaction of metallic particles with gaseous environments
c) A collision or change of the shape of the melted and solidifying particle
d) A dendritic crystallisation in the form of unfilled cavities at the surface of solidified particles not joined with the substrate of further layer
e) A growth of cracks, which are extended into particles or which damage bonds with the substrate and further layers.

2.4.2. Coating thickness

Hogmark and Hedenqvist [67] found that coating erosion resistance decreased with increasing coating thickness. However, it is important to consider coating adhesion to the substrate surface. Particle impact causes a strain build-up in the coating and sub-surface lateral cracks start to occur. The intersection of such cracks leads to coating degradation.

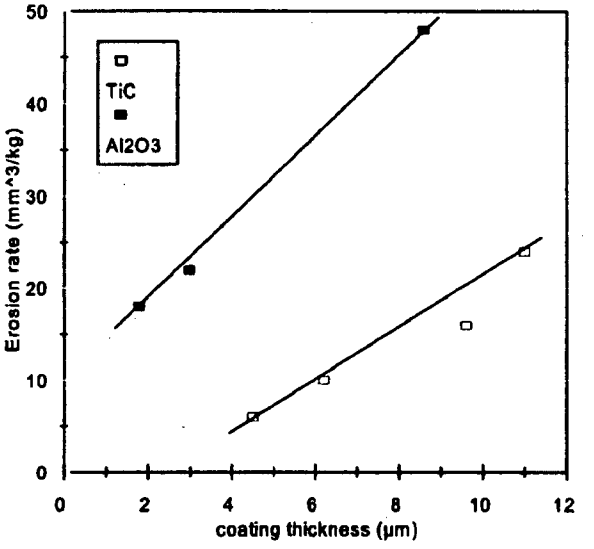

Figure 2.10: *Graph showing a decrease in erosion resistance with increasing coating thickness [67].*

According to Steffens et al [65], a major advantage of thick coatings is that they provide a longer surface life before re-coating is necessary.

2.4.3. Microstructure

Wright and Haywood [64] examined the coatings metallographically and found additional insights for the relative performance of each coating tested. Coatings with a high erosion rate exhibited a high degree of porosity. Oxide content as well as the bond to substrate was also investigated. Oxidising treatments of the coatings produced a very hard, brittle, partially stabilised oxide surface that was extremely erosion resistant.

Olsen et al [68] stated that a fine grain size, low porosity and good adhesion between the coating and the substrate surface will increase the erosion resistance. They also found an increase in coating thickness with an increase in the powder grain size, for similar conditions of application. This increase in grain size will lead to an increase in erosion rates.

2.4.4. Adherence

Joining the coating with the material is largely affected by the preparation of the substrate surface [60]. Mechanical cleaning of the surface is usually accomplished by shot peening, although geometrical characteristics of the surface can be modified. Thus the surface layer is strengthened and activated. A certain roughness of the surface has also positive effects on improving the mechanical joining.

According to Lang [70] surface preparation usually takes one of two forms:

a) Mechanical preparation by lathe turning
b) Grit blasting

The assumption of mechanical joining is filling the surface unevenness on the basis material by particles. However sharp scratches on the substrate surface are undesirable with respect to good coating adhesion to the substrate, since the physical bond requires a perfect contact between two clean surfaces. Adhesion depends on the magnitude and thickness of regions of physical bonds diffusion effects and reactions between particles and surface of the basis material.

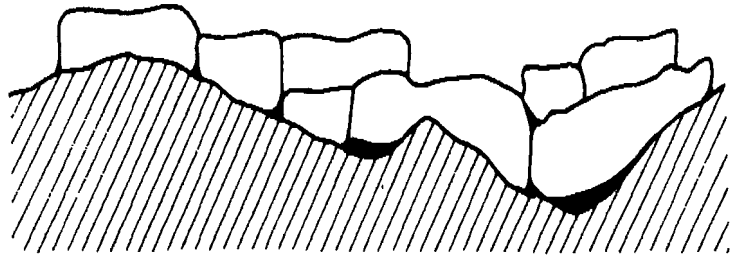

Figure 2.11: *The effect of the surface unevenness after shot peening on the adhesion of the coating [66].*

A good adhesion between the coating and the basic metal or alloy is a decisive condition for their use in practice. The most common test for adhesion is based upon the use of two cylinders, one of which is coated at its one end plane and bonded to the other by a resin, and which is then pulled apart [65].

2.4.5. Residual stresses

Steffens et al [65] found that during the spraying and cooling processes, residual stresses are produced, which may eventually lead to the complete destruction of the coating. The molten-sprayed particles solidify on the cold metal surface and contract during cooling. They are partly prevented from doing this by the adhesion to the metal surface, and thus tensile stresses are produced in the coating. The base metal expands as a result of heat introduced by the sprayed particles causing additional tensile stressing. By cooling the base metal during spraying or by preheating, this additional stress on the coating can be reduced. At high temperatures the yield point of materials are lower so that the resultant tensile stresses can be partially relieved by plastic deformation of the coating. With decreasing temperature, the resistance to deformation and the yield point of the coating rise, and the expansion of the base metal and the extent to which the contraction of the coating is hindered increase until a temperature equilibrium is established. The residual tensile stresses, which can then no longer be relieved by plastic deformation, increase or decrease during the cooling of the composite material depending on the thermal expansion coefficients of the materials involved [65]. The production of internal stresses is mainly due to large temperature differences and different thermal expansion coefficients of the coating and the basis material [66].

2.4.6. Hardness

One of the most important parameters influencing the tribological behaviour of a coated surface is the hardness of the coating and its relationship to the substrate hardness [69]. Hardness is not an intrinsic material property. The hardness is influenced by grain boundary effects, flaws and complex interactions of response behaviours that results in the value measured varying around the mean. Hardness is widely used as a ranking parameter when comparing coatings. The most common hardness measures used for coatings are the VICKERS or the KNOOP microhardness, typically using loads between 10g and 500g.

Davis et al [70] and Hogmark and Hedenqvist [67] noted a decrease in erosion resistance with decreasing coating hardness. Hardness cannot be considered alone when performing characterisation of coated parts. Burnett and Rickerby [71] found that toughness and microstructure must also be considered. Thus hardness cannot be the only factor to be taken into account when ranking coatings in terms of their erosion resistance. Chui and Liou [72] came to the same conclusion.

2.4.7. Surface Roughness

Holmberg and Matthews [69] showed that surface roughness is typically characterised by the profilometer. The main parameters used are the peak to valley height, R_t, and the centre line average value, R_a. Also used is the root mean square value, R_s. The initial surface roughness affects only the early transient stage of erosion and then only when the impacting particles are smaller than the topographical features of the surface [54]. Scattergood [73] found that for relatively smooth surfaces, the initial erosion rate is normally less than the steady-state erosion rate. However when the specimen surface is pre-roughened, the initial erosion rate may be higher than the steady erosion rate, at least for brittle materials. Coating roughness is particularly dependent on the technology of its application, type of material and its grain size [66]. The smaller the initial powder grain size, the smaller the roughness.

2.5. Summary

Two main types of wear processes namely ductile wear and brittle wear, have been reported for solid particle impact. Ductile wear is characteristic of metals and involves plastic deformation of the surface before material loss occurs. Brittle wear on the other hand is characteristic of ceramics and some hard metallic coatings. There is little or no evidence of plastic deformation and material is removed via the propagation and intersection of cracks. Material loss also occurs via a chipping process. These processes were discussed in Section 2.1.

Several factors were found to affect the erosion rate of a material. These included the temperature, the process of erosion-corrosion, mass flux, impact angle, velocity and the erodent. These variables were all discussed in Section 2.2.

Thermal coatings are an effective means of reducing the erosion rate of materials. The various processes of coating application used in industry were reported in Section 2.3. Results obtained for erosion tests on some coating materials by other researchers were also summarised.

The effect of coating variables on erosion rates was discussed in Section 2.4. The variables discussed included the porosity, coating thickness, microstructure, residual stresses, adherence, hardness and the surface roughness of the coatings.

Chapter 3

Experimental procedure

3.1. Materials

3.1.1. Target materials

A range of coatings was selected in the present work for erosion testing, the nominal compositions of which are shown in Table 1. These coatings are being used or are candidate materials for usage in ESKOM for protection against boiler tube erosive wear. All the coatings were applied to a steel substrate using a plasma spraying process, which was discussed, in Section 2.3.2.1. A low carbon alloy steel, HFS620, which is a typical boiler tube steel, was employed as a comparative standard material during erosion testing. The composition of the steel is also shown in Table 1.

All materials were received in the plate form. The prepared specimens had the following dimensions: 20 mm wide, 6 mm thick and 35 mm long and were eroded in the as received state. A hole with a diameter of 1.9 mm was drilled 4 mm from the target surface to accommodate a 1.5 mm diameter K-type thermocouple, which allowed the specimen temperature to be monitored during testing. A typical test specimen (i) can be seen in Figure 3.1.

In addition to the coated flat specimens, a number of coated boiler tubes were also tested in the high temperature erosion apparatus. The machining of a specially designed specimen holder was necessary to carry out such tests. These specimens had a diameter of 32 mm, a thickness of 4 mm and the width was 20 mm. Figure 3.1 shows a typical test specimen (ii), while Figure 3.2 shows the coated boiler tubes from which it has been machined. The coating thickness in these tubes ranged between 200 and 250 μm. Figure 3.3 illustrates the manner in which the coatings have been manually applied to the boiler steel surface.

Coating		Nominal composition
A	***1-004***	*88% WC, 12% NiCr*
B	***1-001***	*88% WC, 12% Ni*
C	***1-005***	*75% CrC_3, 25% NiCr*
D	***5-322***	*25% Cr, 5 % Al, bal. Fe*
E	***5-304***	*28% Cr, 21% Ni, 2% Mn, 0.09 % C, bal. Fe*
F	***5-314***	*75% Cr, 25% Ni*
G	***5-314-6***	*50% Cr, 50% Ni*
H	***502***	*14-18% Cr, 2.5-3.5% Al, bal. Fe*
K	***1-007***	*88% WC, 12% Cr*
L	***5-310***	*27% Cr, 3% Mo, 5% Al, bal. Fe*
STEEL HFS620		*0.1-0.15% C, 0.1-0.35% Si, 0.4-0.7% Mn, 0.03% P, 0.03% S, 0.7-1.10% Ct, 0.45-0.65% Mo, bal. Fe*

Table 1: *The table summarises the nominal composition of the steel and the coatings tested.*

Note

Coatings C, G and H were only applied to flat specimens, while coatings K and L were only applied to boiler tubes. The remaining coatings A, B, D, E and F were applied to both flat specimens and boiler tubes.

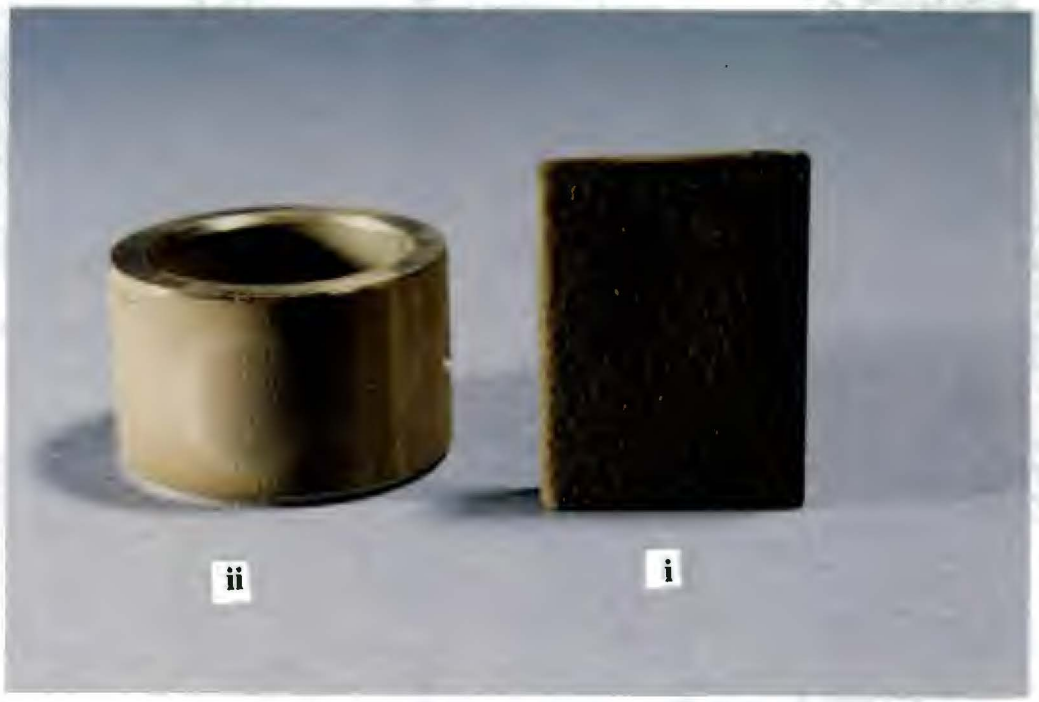

Figure 3.1: *Photograph showing the coated flat and coated boiler tube specimens for erosion testing in the HTER.*

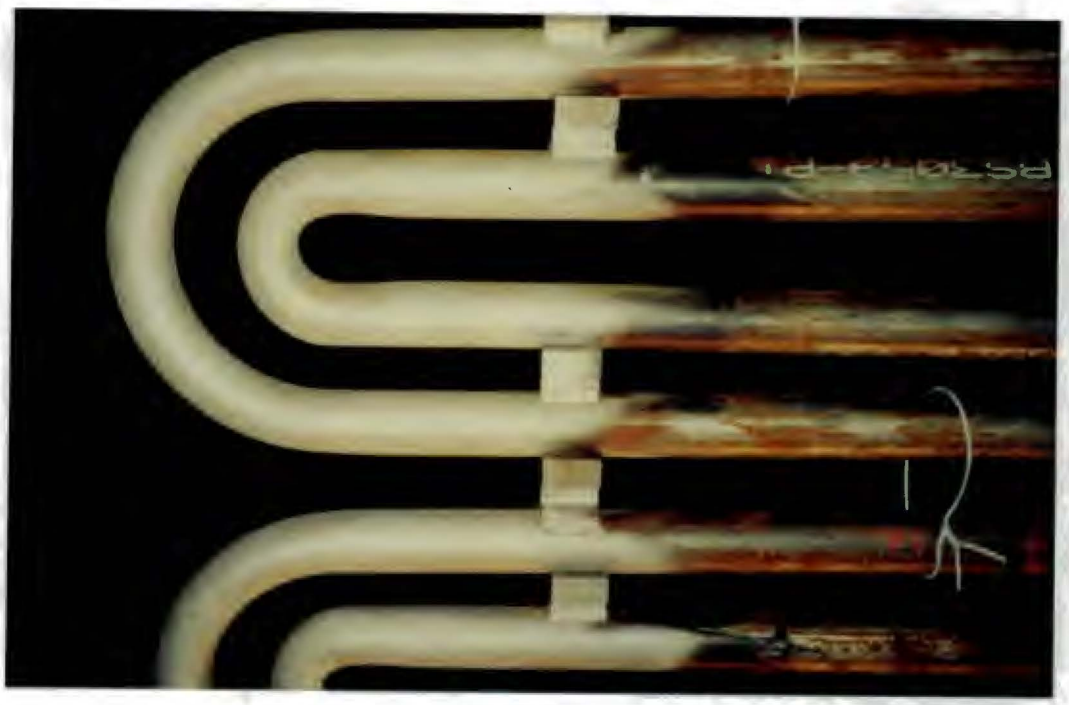

Figure 3.2: *Photograph showing the partially coated boiler tube from which the test specimen has been machined.*

***Figure 3.3:** Photograph showing the manual process of flame spraying. The coating applied to the boiler steel surface has a thickness of approximately 250 μm.*

3.1.2. Erodent

Silicon oxide or silica sand (SiO_2) was used as the erodent in the erosion tests. The SiO_2 grit was obtained from a local manufacturer and sieved to the desired size range, i.e. 63 – 106 μm. Ash particles in the size range 63 – 106 μm are predominant in the region of high erosion in coal fired power plants. Silica sand was preferred to ash as the erodent since ashes do not lend themselves to easy and accelerated testing on the high temperature erosion apparatus. Ashes contain high quantities of silica, which is the most erosive component of fly ash. It was shown in previous work that virgin silica could be used as a substitute with no significant comparative changes in the results obtained [7]. Another reason for using silica sand was the difficulty encountered in sieving ash particles to obtain the above mentioned size range. The SiO_2 particles are rounded as shown in Figure 3.4.

Figure 3.4: *SEM micrograph showing the rounded nature of SiO_2 erodent. Porosity and nodules can be seen on the surface of the SiO_2 erodent.*

3.2. Apparatus

3.2.1. The High Temperature Erosion Rig (HTER)

The High Temperature Erosion Rig (HTER) was designed and build to simulate the actual boiler environment conditions in which erosion of tubes is a serious problem. The erosive test conditions are presented in Table 2, Section 3.3. A schematic of the erosion rig is shown in Figure 3.5.

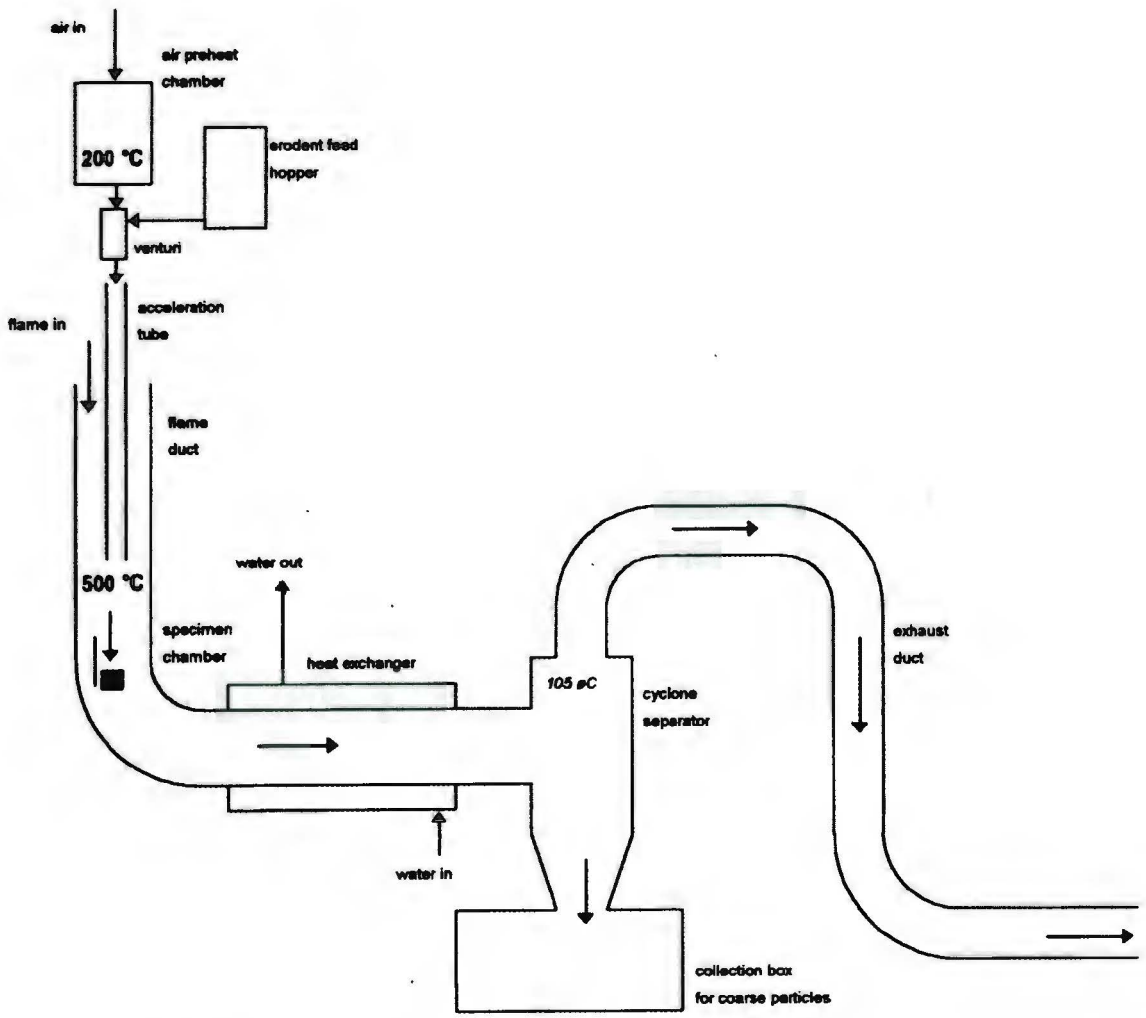

***Figure 3.5:** Diagram of the high temperature erosion rig (HTER) [74].*

Silica particles (Figures 3.4) are introduced into the erodent feed hopper. Compressed air is fed into a preheating chamber, which heats the air to a temperature of 200°C using "cartridge" heating elements. The compressed air is fed through a venturi, creating a vacuum

in the feed line. Adjusting the pressure of the air controls the velocity of the erodent particles in the air stream. A velocity of 24 $m.s^{-1}$ was used for testing at 40° impact in all the cases. The erodent carrying tube passes through a duct and is heated by a propane burner. The heat from the burner heats both the down tube and the specimen in the specimen chamber. A cover plate seals the specimen chamber and prevents the gas mixture from escaping to atmosphere [74]. Figures 3.6 – 3.11 show the apparatus in photographic form.

Figure 3.6: *Photograph of the upper half of the HTER.*

Figure 3.7: *Photograph of the erodent feed hopper.*

A: Compressed Air, **B**: Preheating Chamber, **C**: Erodent Feed Hopper, **D**: Grooved Turntable, **E**: Venturi

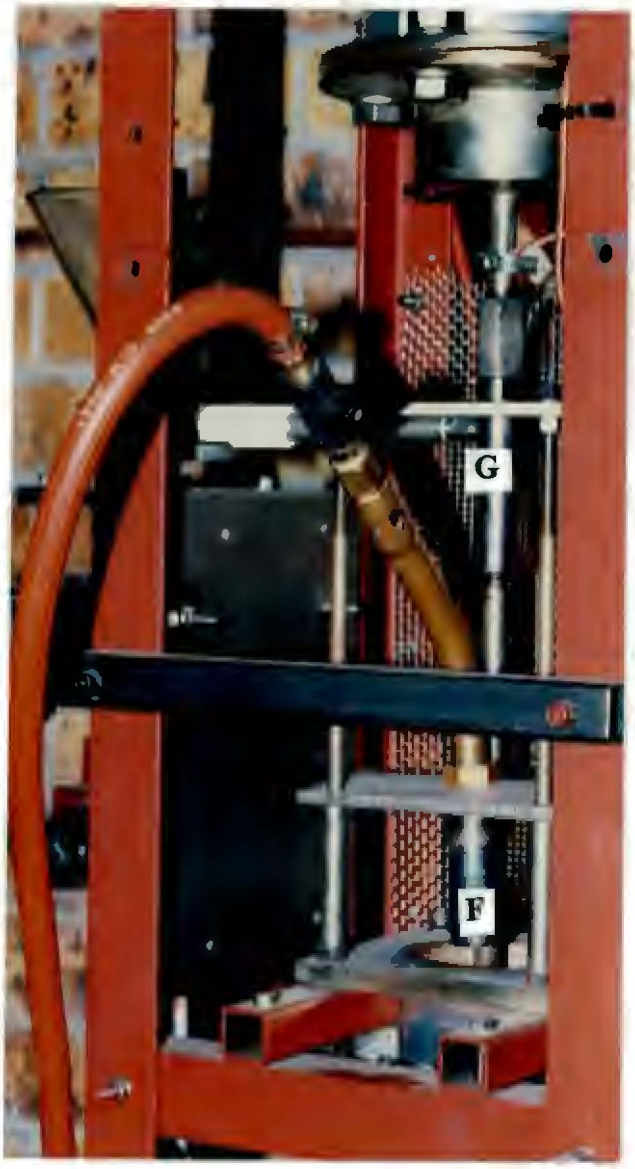

Figures 3.8: *Photograph of the propane burner.*

Figure 3.9: *Photograph of the specimen chamber.*

F: Propane burner, **G**: Acceleration tube, **H**: Specimen chamber

Figure 3.10: Photograph of coated specimen on specimen stage.

I: Cover Plate, **J**: Alumina Specimen Stage

Figure 3.11: Photograph of coated boiler tube specimen on specimen stage.

K: Specimen Holder for Coated Specimen

3.2.2. Calibration of the HTER

It was necessary to calibrate the high temperature erosion rig to achieve an experimental mass flux of 0.21 $kg.m^{-2}.s^{-1}$. The calibration was carried out at 400°C. This calibration was achieved by passing a measured mass of erodent (5 g) through the erodent feed hopper onto the turntable and hence into the venturi. The mass flow is controlled by adjusting the velocity of the turntable. The time was noted and converted to seconds after which the flux was calculated.

Note

The following relationships were used to determine the flux:

$$\text{mass feed rate} = \text{mass} \div \text{time}$$

units

mass = kilogram(kg), time = seconds(s)

The diameter of the acceleration tube through which the erodent passes is 9.6 mm. Therefore,

$$\text{Cross sectional area} = \Pi \times (0.096/2)^2$$
$$= 7.24 \times 10^{-5} m^2$$

Mass flux = mass feed rate ÷ cross-sectional area

See also Appendix A for the complete operating procedure of the high temperature erosion rig (HTER).

3.3 Experimental matrix

The following experimental conditions were used during erosion testing:

Temperature	400°C
Mass flux	0.21 $kg.m^{-2}.s^{-1}$
Velocity	24 $m.s^{-1}$
Impact angle	40°
Erodent	Silica sand (SiO_2)
Erodent size	63 - 106 μm
Surface finish	As received
Mass of erodent per test	50 g

Table 2: *The table summarises the experimental matrix used for erosion testing.*

These conditions were chosen to simulate the actual conditions in the boiler plant as detailed below.

i) Temperature: Boilers are found to be most vulnerable to erosion damage at a temperature of 400°C [33, 34].

ii) Velocity: Erosion tests were carried out at 24 $m.s^{-1}$, which is at the high end of the range of velocities most frequently found in boilers at a temperature of 400°C [7]

iii) Mass flux: A mass flux of 0.21 $kg.m^{-2}.s^{-1}$ is typically found in the economiser regions of the boilers at 400°C [42, 43, 65].

iv) Impact angle: An angle of 40° was chosen because it was found to be the angle at which maximum material loss occurs for boiler tube material [4, 6, 21].

v) Erodent: Silica sand was chosen as the erodent, because of the difficulty encountered to accelerate fly ash on the high temperature erosion apparatus. Silica was also chosen because it was difficult to obtain the fly ash erodent size range indicated in the table above. SiO_2 is the most erosive component of fly ash [7].

vi) Erodent size: Fly ash in the size range 63 to 106 μm is predominantly found in boiler plants.

3.4. Testing method

3.4.1. General method

Initially the apparatus was switched on and left to warm up for 40 minutes to achieve maximum pre-heat. During this period the erodent mass for testing was measured on a Mettler PC440 balance. The prepared specimens were cleaned in alcohol in an ultrasonic bath and weighed on a Mettler balance to an accuracy of 0.01g. The surface roughness was measured using a Taylor-Hobson Surtronic 3P stylus profilometer. The specimen was then placed on the insulating alumino-silicate fibre board and mounted on the AISI 316L stainless steel specimen stage (See Figure 3.10, Section 3.2.1). The specimen was secured in the specimen chamber.

It was necessary to check whether the cooling system was functioning properly before the gas tap was opened and the propane gas flame ignited. The apparatus took about 10 minutes before stabilising to within 5°C of the control temperatures. The temperature was noted and the erodent was fed through the hopper. A stopwatch was used to monitor the length of the erosion test. When all the erodent has run out the stop-watch was stopped and a second temperature reading was taken. The specimen could only be removed once the specimen temperature has dropped to about 150°C. The specimen was then air cooled, cleaned in alcohol and blow dried.

Erosion of the specimens was measured by recording the weight loss of the samples on a Mettler balance to an accuracy of 0.01 mg. Another roughness test was then performed. Erosion testing of the specimens was continued until at least three constant weight loss measurements were obtained. The total time of erosion testing was approximately 300 minutes.

3.4.2. Flow chart of erosion procedure

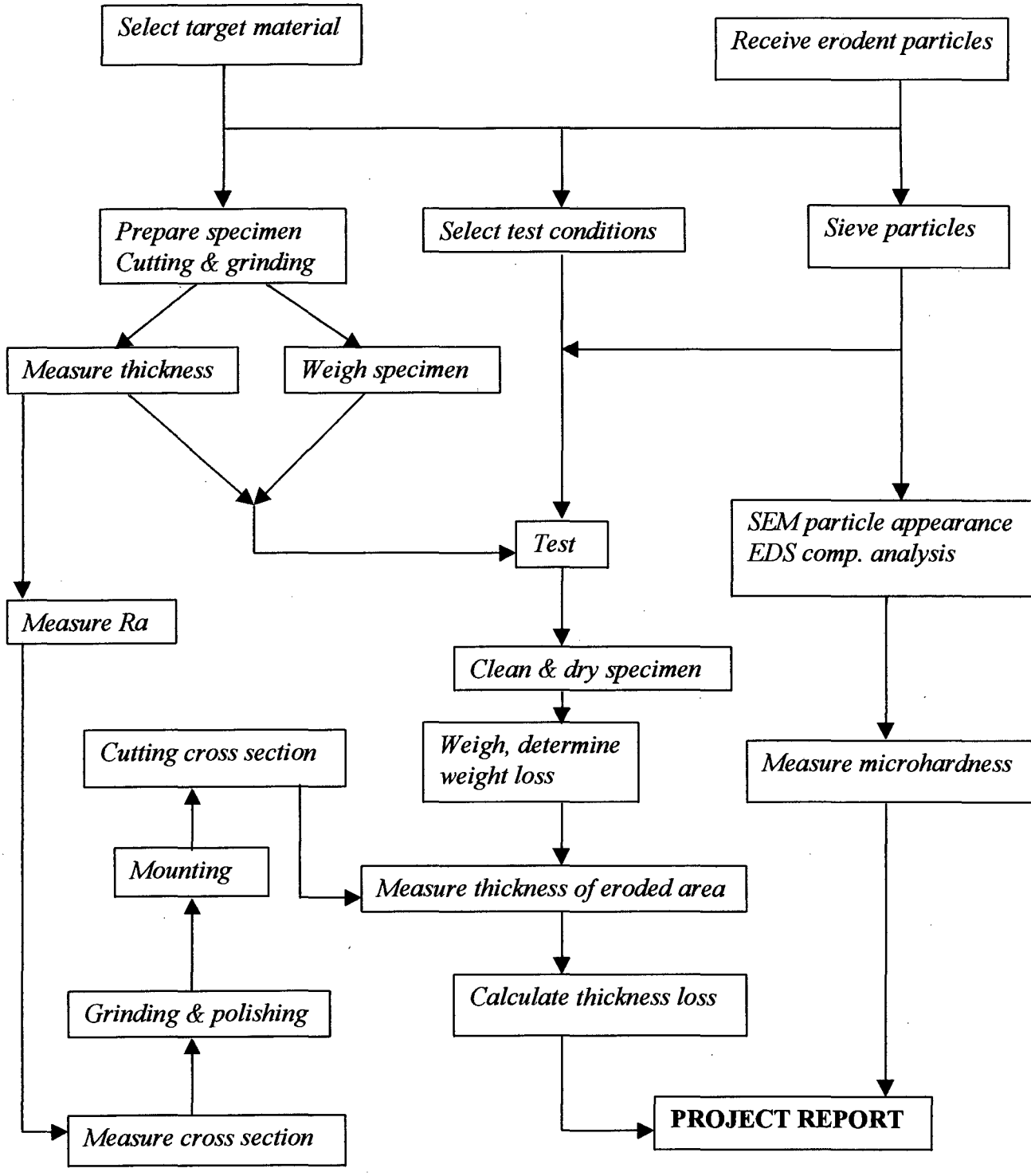

Typical Flow Chart of Erosion Process

The chart is a representation of the procedure that was followed during high temperature erosion testing.

3.5. Determination of the erosion rates

Erosion tests were conducted to obtain the steady erosion rate of eight commercial thermally sprayed protective coatings. All the coatings were tested under similar conditions, shown in Table 2, in the high temperature erosion rig. Figure 3.12 shows a typical plot of the cumulative mass loss versus the cumulative erodent mass. The linear portion of the slope was used to determine the steady erosion rates as the mass loss per mass of erodent, the results of which are presented in Table 3, Section 4.1.

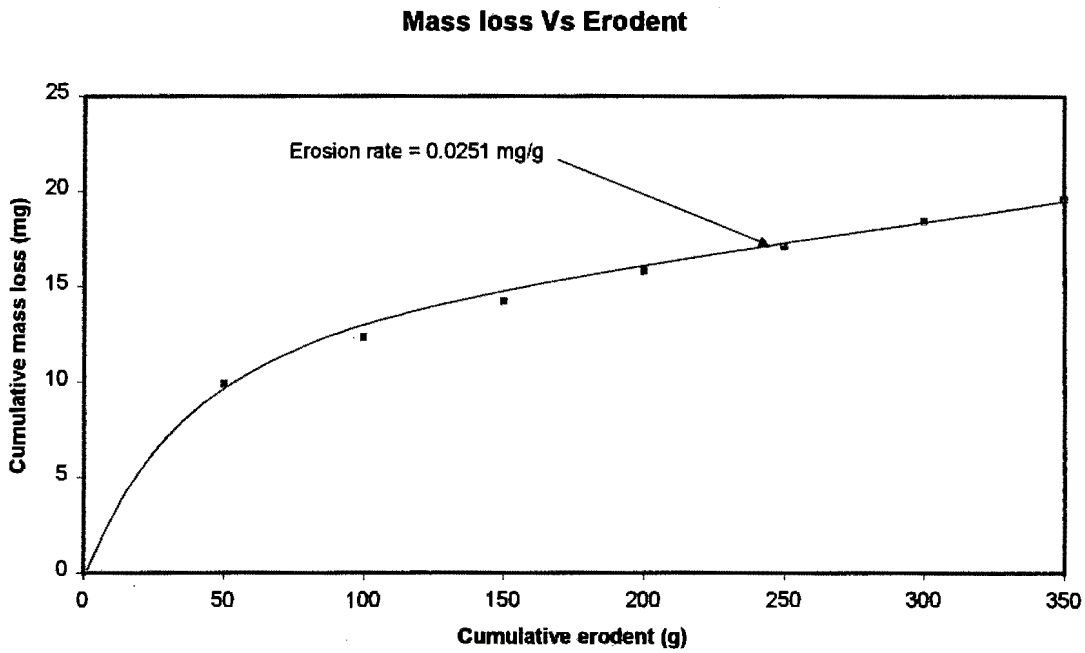

Figure 3.12: *Graph of cumulative mass loss Vs cumulative erodent for coating A. The erosion rate is determined from the linear portion of the curve.*

The erosion rates of the coatings and the boiler steel were also determined as the volume loss per mass of erodent. This was achieved by dividing the slope of the graph in Figure 3.12 by the density of the coating. The density of each coating material was calculated using the chemical content and the density of the elemental constituents as shown below.

Example: Coating A

Element/Compound	*metal %*	*density(g/cm^3)*	*% × ρ*
WC	*88 (87.8)*	*15.77*	*13.88 (13.85)*
Ni	*12 (12.2)*	*8.36*	*1.06 (1.02)*
Coating density			*14.94 (14.87)*

Thus the nominal density of coating A used in calculations was 14.94 g.cm^{-3}. The actual chemical composition and coating density are given in brackets. The same procedure was followed to calculate the density of the remaining coatings and the basis steel. Therefore,

$$\textbf{Erosion rate of A} = (0.0251) / (14.94 \times 1000) = 1.69 \times 10^{-6}\ \textbf{cm}^3/\textbf{g}$$

Although it can be assumed that the actual coating composition will be different to the nominal analysis, any minor differences were not considered to have a significant effect on these density values especially given that the coating composition is likely to vary within the coating. For example, a chemical analysis of coating A showed less than 1 % difference in the elemental analysis between the nominal and actual compositions. The erosion rate and the density of the boiler tube steel were obtained in a similar manner.

3.6. Microscopy

Metallurgical examination was carried out on cross-sectioned as received and worn specimens. This was accomplished by mounting the specimens in epoxy resin, followed by grinding on different grits of carborudum ranging from 1200 to 80 μm. The specimens were then polished on a 3, 1 and 0.25 μm diamond impregnated pads and viewed under the Reichert MeF3A optical microscope. Micrographs were taken of the microstructure.

Specimens were also mounted onto aluminium stubs and coated with gold-palladium to ensure electrical conductivity. The cross-sectioned specimens were then viewed under the

Cambridge S200 scanning electron microscope (SEM). The chemical compositions of the coatings were determined by energy dispersive analysis under the SEM.

Worn specimens were cleaned in ethanol before being mounted onto aluminium stubs coated with gold palladium and inserted into the scanning electron microscope (SEM) for examination. Specimens were viewed at 25 kV, which gave a good resolution. Erodent particles (silica sand) were also viewed under the SEM at a potential difference of 25 kV. At settings higher than this the particles became electrostatically charged resulting in florescence. These particles were also mounted onto an aluminium stub and coated with gold-palladium to ensure electrical conductivity before micrographs were taken under the SEM.

3.7. Surface roughness testing

The surface topography of the coatings was determined using a Taylor-Hobson Surtronic 3P stylus profilometer (Figure 3.13). The fine stylus is dragged smoothly and steadily across the surface, which rises and falls as it travels across the surface. Its vertical displacement is converted by a transducer into an electrical signal, which is amplified. In this work, the quoted measure of roughness is the average roughness, Ra, which is the arithmetic mean deviation of the surface height from the mean line through the profile. Equal areas of the profile lie above and below this mean line. The roughness was taken as the average of ten measurements. (See also Appendix C)

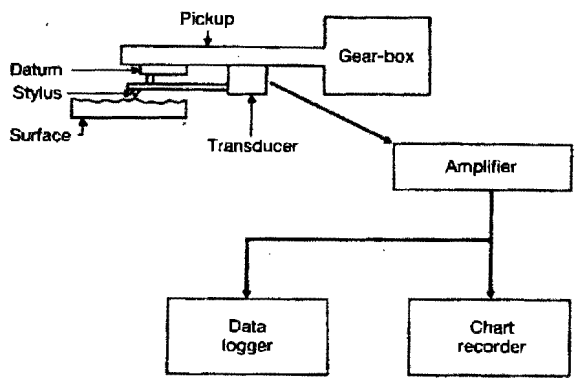

***Figure 3.13:** Diagram of the stylus profilometer [75].*

3.8. Microhardness testing

The hardness of the coatings was measured using the Matsuzawa microhardness tester. The specimens were mounted in epoxy resin and polished before the Vickers hardness was determined at a load of 50 gf. A total of five constant measurements were taken before the average was recorded as the hardness of the steel or for a particular coating.

3.9. Porosity measurements

The porosity content of the coatings can be determined semi quantitatively by areal analysis, lineal analysis or point counting. In this work, lineal analysis was employed to determine the porosity content in the microstructure of the coatings. Up to 80 random lines were drawn on photomicrographs and the intercept length of a porous region was measured. The porosity fraction was then determined using the relation

$$V_v = L_c/L_t.$$

V_v = porous volume fraction, L_c = intercept length a of porous region, L_t = total length of the line

In addition, the porosity fraction of the coatings were also determined by image analysis using the Joyce Loebl Mini Magic Scanner. The apparatus distinguishes between contrasting areas (usually black and white) in an image. The porosity content in the coating microstructure was determined from black and white negative films.

Chapter 4

Results

4.1.1. Erosion tests on as received material

All the materials were tested under similar conditions, as outlined in Section 3.3. The results of the erosion tests on the eight as received coatings showed that the volume loss of material with increasing time of erosion was not constant. Initially, the rate of material loss was found to be high which decreased as the erosion test proceeded until a constant rate of volume loss with erodent mass was achieved. Figure 4.1 shows the typical behaviour of these coatings when plotting cumulative volume loss against cumulative erodent mass. The determination of the erosion rate was taken from the slope of the steady state portion of these curves for the various coatings as shown in Section 3.5, Figure 3.12. The results for all the coatings are shown in Table 3.

Figure 4.2 demonstrates that the behaviour of the boiler steel was different. There was no transient period before steady state conditions were achieved and a plot of cumulative volume loss with cumulative mass of erodent was linear throughout the test. Table 3 also contains the calculated erosion rate for this steel which is also seen plotted in the form of a histogram in Figure 4.3.

Coating	*Erosion rate (mg/g)*	*Density (g/cm^3)*	*Erosion rate ($cm^3/g \times 10^{-6}$)*
A	*0.0251*	*14.94*	*1.69*
B	*0.0484*	*14.93*	*3.24*
C	*0.0259*	*6.88*	*3.76*
D	*0.0499*	*7.52*	*6.63*
E	*0.0730*	*7.95*	*9.18*
F	*0.0722*	*7.83*	*9.22*
G	*0.0992*	*8.15*	*12.2*
H	*0.1066*	*7.62*	*14.0*
Steel	***0.0444***	***7.80***	***5.69***

Table 3: *The table summarises the erosion rates and densities of the different coatings and the basis steel.*

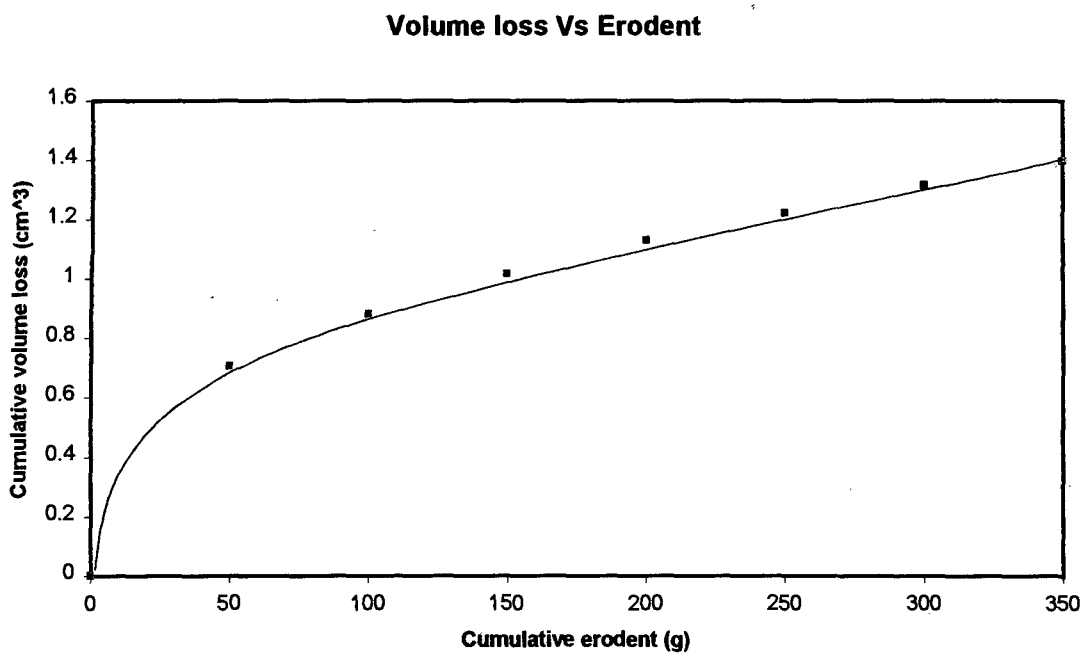

Figure 4.1: *Plot of cumulative volume loss Vs cumulative erodent for coating A. The erosion rate was determined from the slope of the steady state portion of the curve as shown in Figure 3.12.*

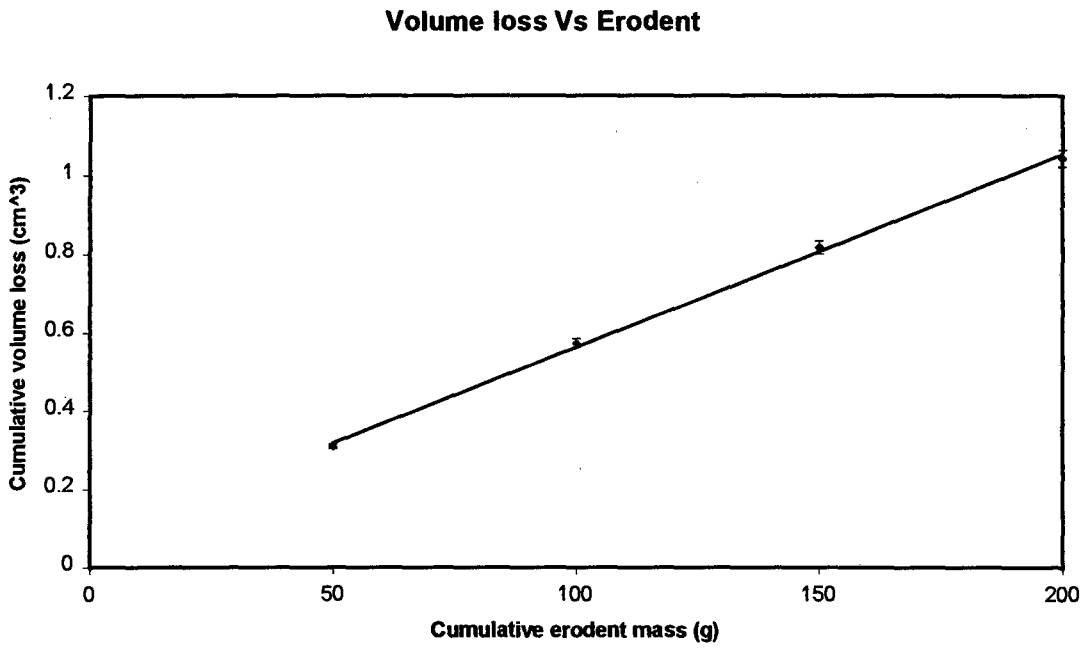

Figure 4.2: *Plot of cumulative volume loss Vs cumulative erodent for the boiler steel. The curve shows no transient period and the erosion rate is determined from the slope of the straight line.*

The error bars indicate that consistent results were obtained for the volume loss measurements during the period of erosion testing for the boiler tube steel specimen. The calculated error was determined to be less than 2 %.

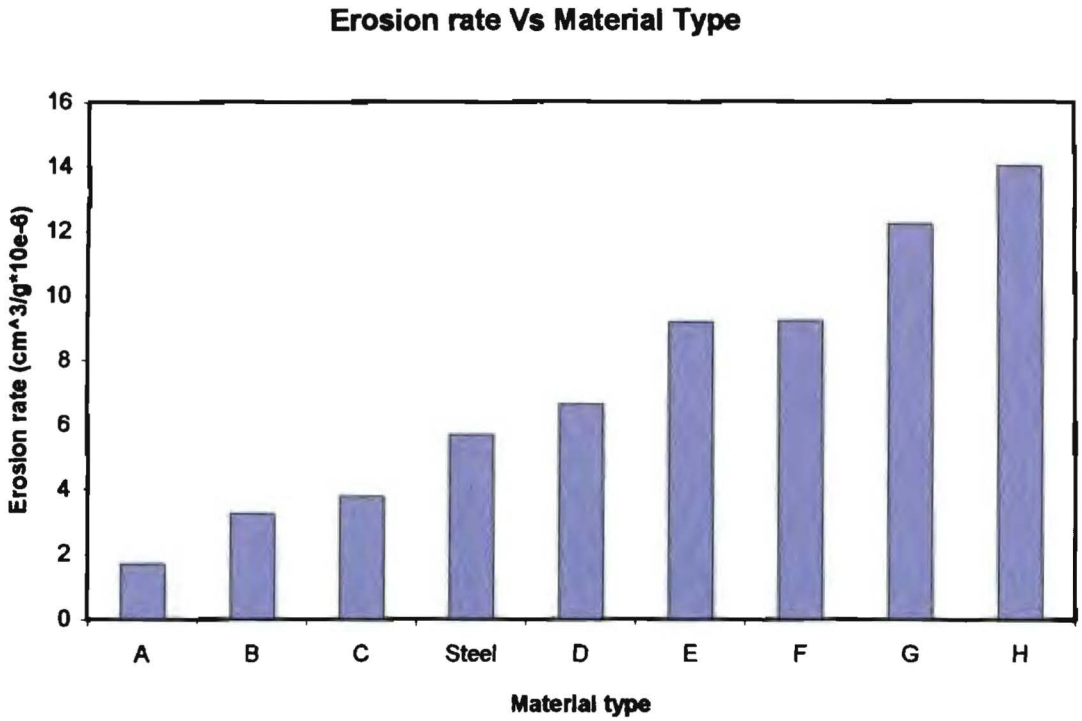

Figure 4.3: *The histogram compares the erosion rate of each coating and the boiler steel.*

The results show that there is a wide divergence in the erosion behaviour of the various types of coatings. For example, the erosion rate shown by coating H is almost eight times higher than that of coating A. More surprising, only three of these eight coatings performed better than the boiler steel under the conditions of testing. The steel was found to have an erosion resistance more than double that of the worst coating H.

4.1.2. Erosion tests on ground specimens

The as received coatings were all found to have different initial surface roughnesses. The values of surface roughness Ra varied from 4.25 μm for coating C to 21.65 μm for coating H. The effect of this surface roughness on the erosion rate of the coatings was investigated by grinding coated specimens to a surface roughness Ra between 2.04 μm and 2.15 μm approximately similar to that of the as received boiler steel plate, and testing it in the HTER. Erosion tests were performed in a similar manner as previously described in Section 3.4.1. The erosion tests were only carried out on the three coatings A, B and C that outperformed the steel substrate in the first set of tests on the as received material. The results are shown in Table 4.

Coating	*As Received Initial R_a*	*Ground Final R_a*	*As Received Initial ER ($cm^3/g * 10^{-6}$)*	*Ground Final ER ($cm^3/g * 10^{-6}$)*
A	*5.83*	*2.04*	*1.69*	*1.54*
B	*4.25*	*2.10*	*3.24*	*2.80*
C	*7.69*	*2.15*	*3.76*	*4.11*
Steel	***1.9***	***1.9***	***5.69***	***5.74***

***Table 4:** The table summarises the average surface roughness before grinding and after grinding. Also shown is the erosion rate of the specimens before and after grinding.*

It was found that by grinding the surface of the coatings prior to testing resulted in a constant rate of material loss during the period of testing. No transient period was apparent before steady conditions were achieved. This is illustrated for coating B in Figure 4.4. This result was similar to that shown by the as received steel in the first series of tests. Furthermore it was found that the measured erosion rates for two of the coatings namely A and C together with the steel sample did not change significantly, i.e. less than ± 10 %, whilst the erosion rate for coating B decreased by 13.5 %. The comparative erosion rates of the as received material and ground material is shown in Figure 4.5.

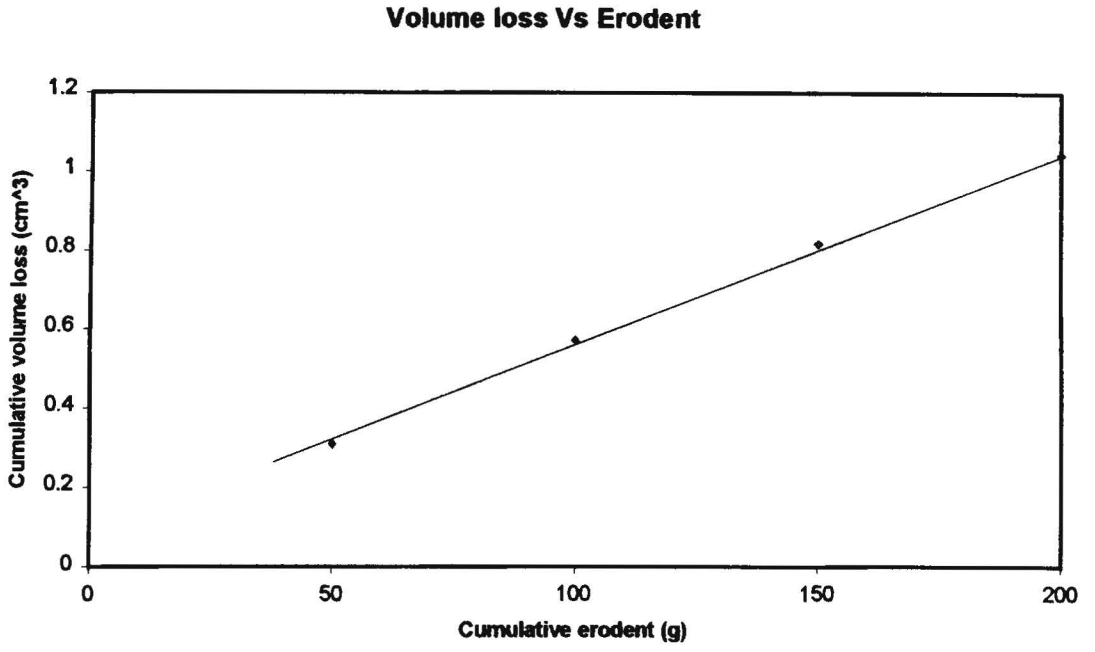

Figure 4.4: *Plot of cumulative volume loss against cumulative erodent mass for coating B shows no transient period.*

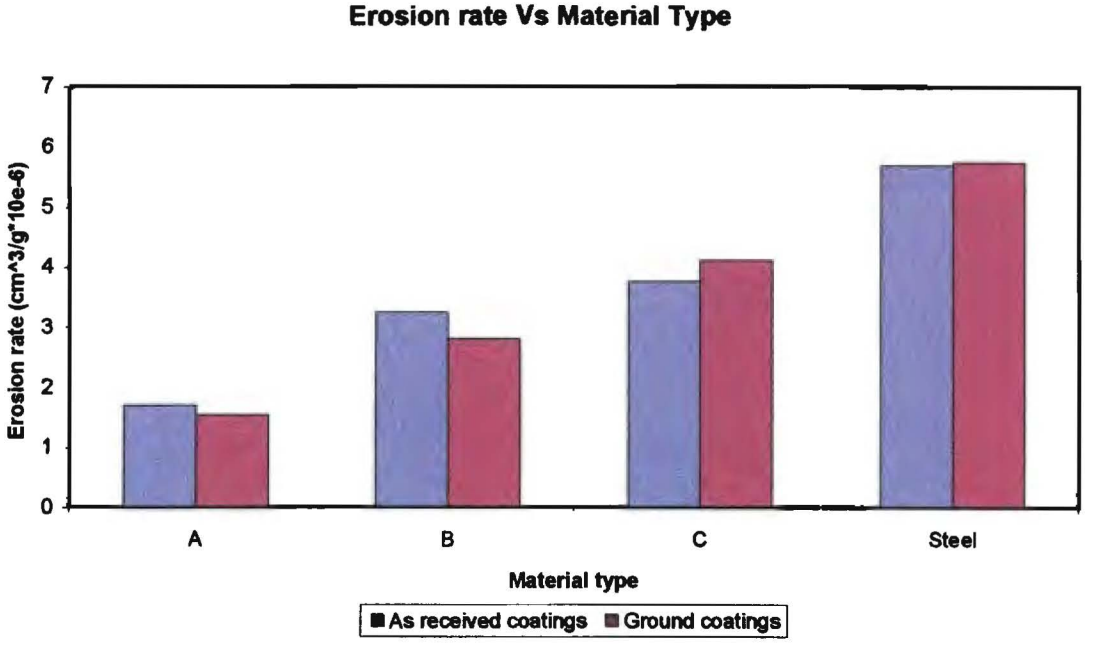

Figure 4.5: *Histogram comparing the erosion rates of coatings and steel before and after grinding.*

4.1.3. Erosion tests on coated boiler tubes

Seven coated tubes were eroded, five of which had similar compositions to those of the flat specimens as summarised in Table 1, Section 3.1.1. This was done in order to compare their erosion rates with the erosion rates of coated flat specimens A holder for the high temperature erosion rig was specially designed for this purpose. The tests were carried out using the same erosive conditions as those for the flat specimens. The results of these tests are summarised in Table 5 and were obtained from the steady state portion of the material volume loss versus cumulative erodent mass graph. All the coated, as received specimens showed an initial transient period similar to that found for the as received coated flat specimens as previously detailed.

Coating		Erosion rate (mg/g)	Density (g cm^{-3})	Erosion rate (cm^{3}g^{-1}10^{-4})
A	*1-004*	*0.0213*	*14.94*	*1.43*
B	*1-001*	*0.0197*	*14.93*	*1.32*
K	*1-007*	*0.0234*	*14.78*	*1.58*
D	*5-322*	*0.0557*	*7.52*	*7.41*
E	*5-314*	*0.0609*	*7.83*	*7.78*
F	*5-304*	*0.0578*	*7.95*	*7.27*
L	*5-310*	*0.0552*	*7.58*	*7.28*
Steel		*0.0252*	*7.80*	*3.23*

***Table 5:** Table summarising the erosion rates and densities of the coated boiler tube specimens.*

The erosion rates obtained using the cylindrical test pieces exposed to the erodent stream were found to be lower when compared to similar coated flat specimens. The decrease in erosion rates ranged from 59 % for coating B to 15 % for coating A. The decrease recorded for steel was 43%. Figure 4.7 shows the results of this series of testing in the form of a histogram. It can be seen that only three of these coatings namely A, B and K outperformed the boiler steel with erosion rates less than 50 % of the steel whilst the other four coatings have erosion rates over twice that of the steel sample. It should be noted however that the spread of erosion rates

spread of erosion rates for these coatings at 5 times is lower than that obtained for similar coated flat specimens of 8 times between the highest and lowest erosion rates.

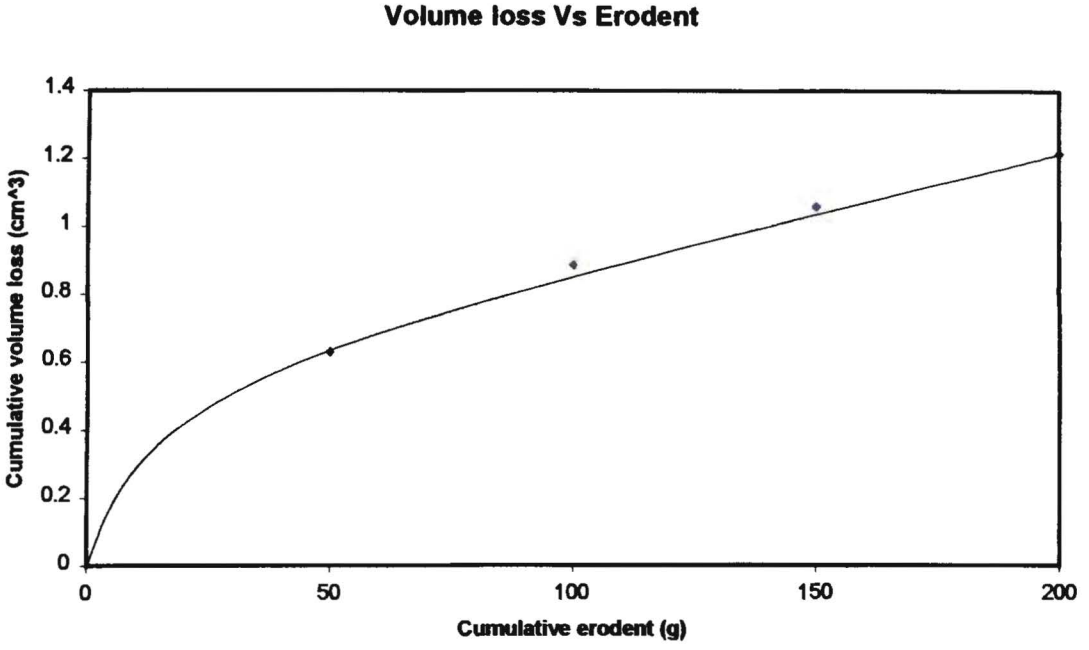

Figure 4.6: *Plot of cumulative volume loss Vs cumulative erodent for a coated boiler tube specimen shows a transient period before reaching steady volume loss.*

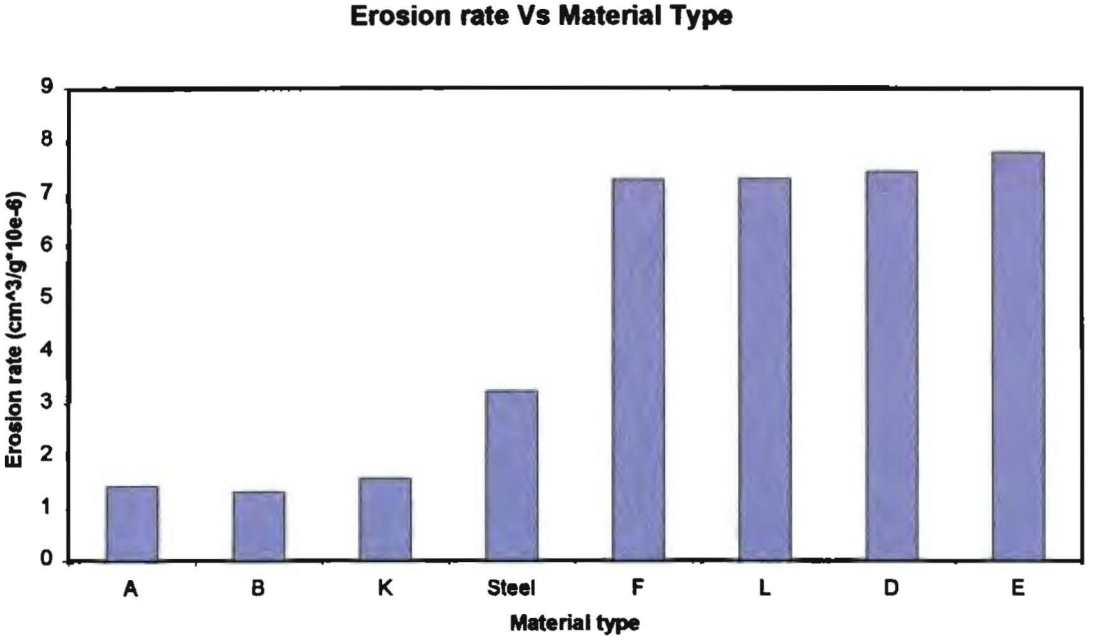

Figure 4.7: *Histogram comparing the erosion rate of the coated boiler tubes with the erosion rate of the boiler steel.*

4.2. Velocity effect on the erosion rate

Erosion tests were performed on one coating E, to determine the effect of impact velocity on its erosion rate. Erosion tests were carried out at 20, 24, 30, 40 and 50 $m.s^{-1}$. The experimental matrix summarised in Section 3.3 was followed. The experimental data presented in Table 6 shows that the erosion rate increased when the impacting particle velocity was increased. The erosion rate increased 33 times from the lowest testing velocity (20 $m.s^{-1}$) to the highest (50 $m.s^{-1}$).

Velocity ($m.s^{-1}$)	*Steady erosion rate (mg/g)*	*Erosion rate ($cm^3/g*10^{-6}$)*
20	*0.0172*	*2.21*
24	*0.0730*	*9.36*
30	*0.2446*	*31.3*
40	*0.4854*	*62.2*
50	*0.5732*	*73.5*

***Table 6:** The table shows that the erosion rate increased with increasing impact velocity.*

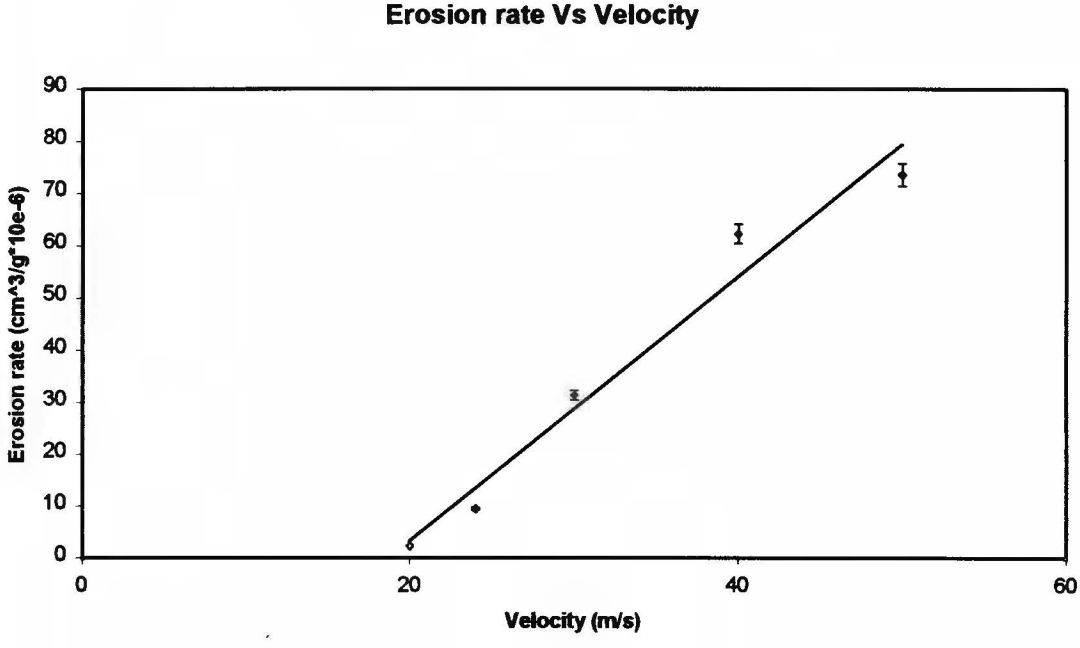

***Figure 4.8:** Velocity effect on coating E erosion rate.*

The erosion rate at the different velocities is shown graphically in Figure 4.8. The error bars indicate the uncertainty in the value obtained. The error is small when testing at lower velocities but increases when the tests were performed at higher impact velocities. The solid line represents a power law curve fit of the experimental data. The velocity exponent obtained from the slope of the graph was determined to be 1.97.

4.3. Micrographs and Quality of the coatings

Considerable variability was found in the microstructure of all the coatings. The microstructure of coating A shows that the WC particles are very fine and uniformly dispersed throughout. Furthermore the porosity content is low and relatively uniform across the coating thickness. This is illustrated in Figures 4.9 and 4.10. Two different phases can be distinguished from the SEM micrograph in Figure 4.10. The coating is typically that expected of good thermally sprayed coatings.

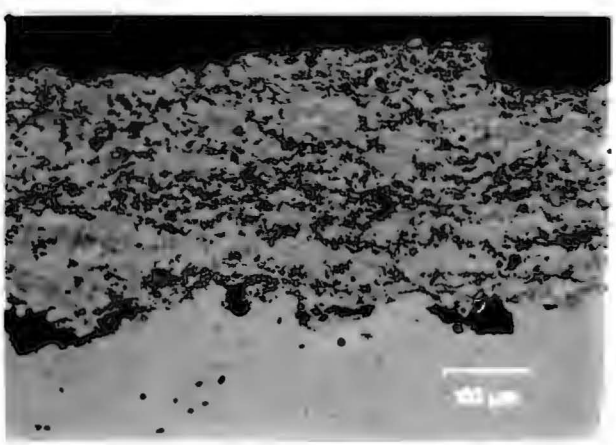

***Figure 4.9:** Optical micrograph showing the microstructure of coating A.*

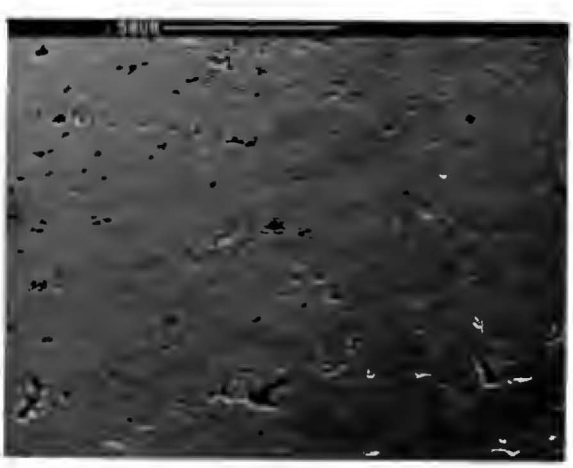

***Figure 4.10:** SEM micrograph depicting the microstructure of coating A and showing a uniform composition distribution. Porosity can also be observed.*

A similar homogeneous microstructure was found in coating B based on tungsten carbide (WC) as shown in Figure 4.11.

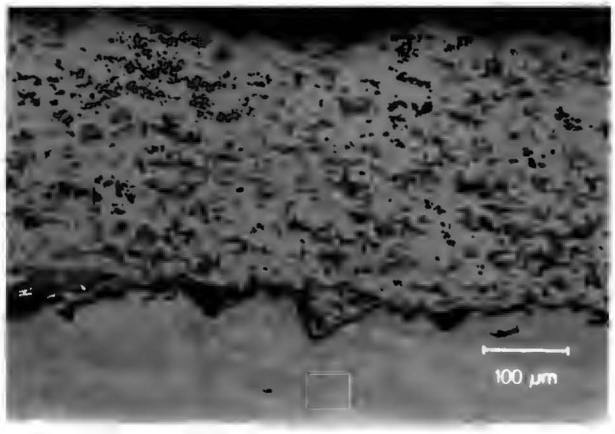

***Figure 4.11:** Optical micrograph showing the microstructure of coating B.*

This is in contrast with coatings D, E and H where different phases were clearly observed. The porosity content was found to be relatively high, coarse and in the case of H not uniformly distributed. The following figures illustrate this.

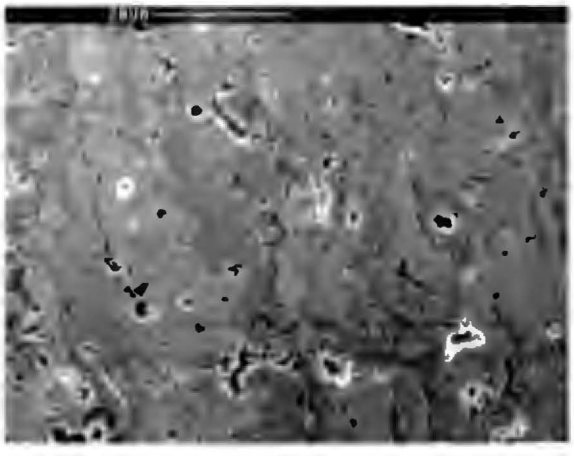

***Figure 4.12:** SEM micrograph of coating D showing a multiphase microstructure and porosity.*

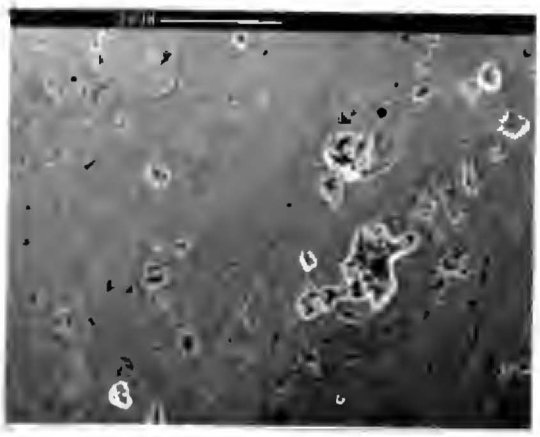

Figure 4.13: *SEM micrograph showing the microstructure of coating E consisting of more than one phase. Porosity is also present.*

The phase composition of the coating H is indicated on the SEM micrograph in Figure 4.14. The micrograph shows that the coating contained three different phases and porous regions.

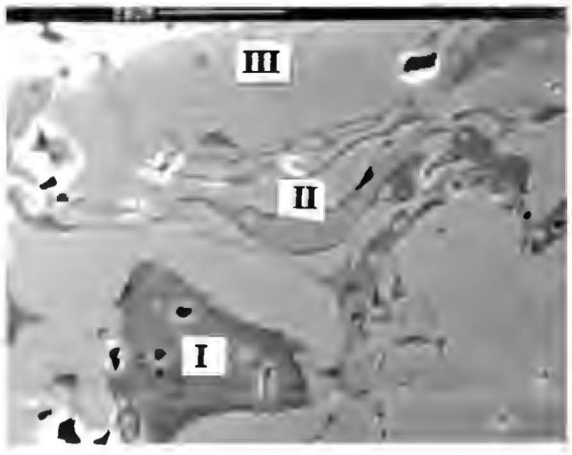

Figure 4.14: *SEM micrograph of coating H showing two distinct phases and porosity.*

I = Cr rich areas, II = Al rich areas, III = Fe rich areas

The microstructures of coatings G and H suggests that these coatings are completely unacceptable for usage against erosion protection because of the high porosity content and the lack of interparticle bonding. The micrographs indicate these defects in the microstructures.

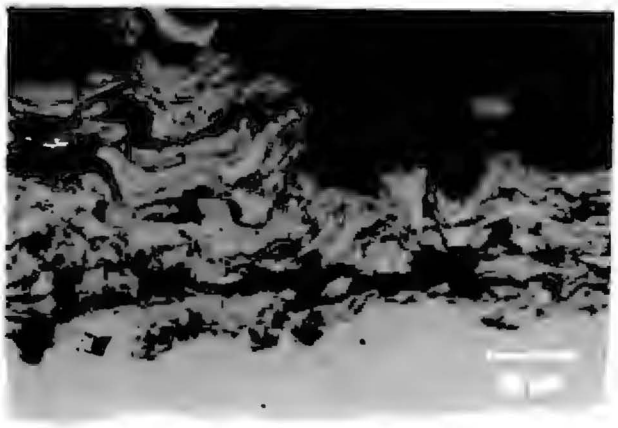

***Figure 4.15:** Optical micrograph showing the microstructure of coating G.*

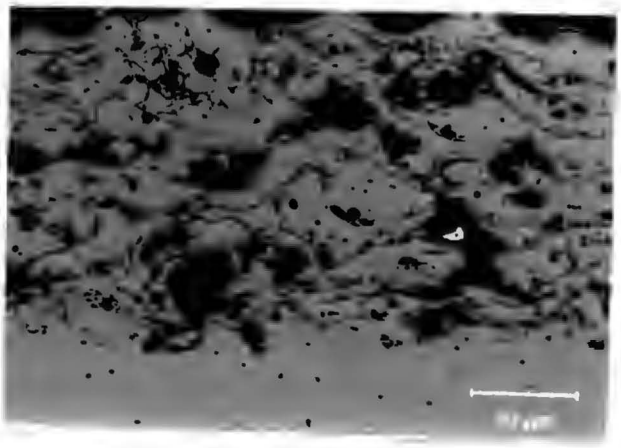

***Figure 4.16:** Optical micrograph showing the microstructure of coating H.*

Whilst coatings C, E and F were found to have a uniform microstructure in terms of adherence and porosity, loose particles were observed on the surface of these two coatings. These are not indicative of the high quality coatings, which are generally produced via the plasma spraying process. Figures 4.17, 4.18 and 4.20 show these loose particles (indicated by the arrows) on the surfaces of these coatings. Figure 4.19 is a SEM micrograph and show how the powder used in the spraying process has only partially melted.

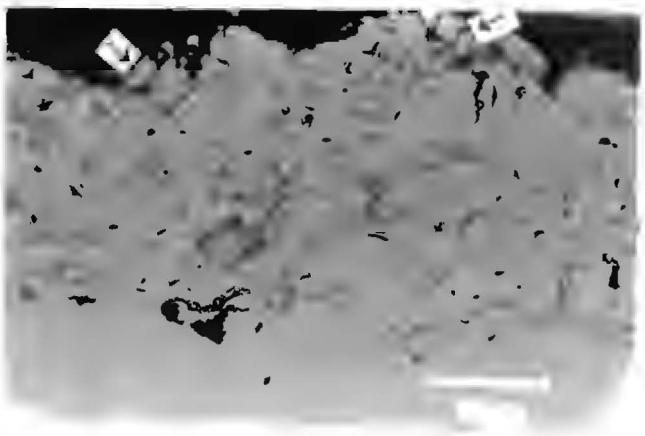

***Figure 4.17:** Optical micrograph showing the microstructure of coating C. Loose particles can be seen on the surface of the coating.*

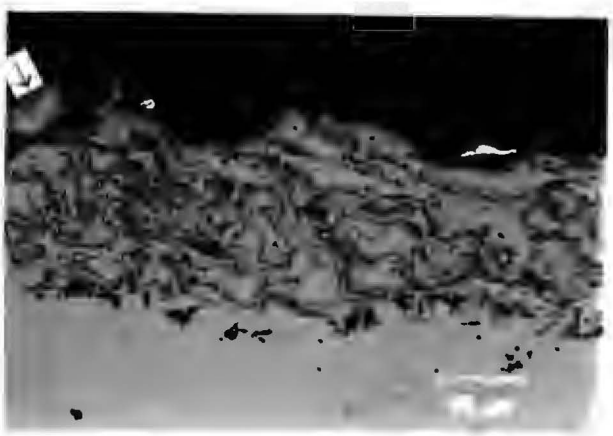

***Figure 4.18:** Optical micrograph showing the microstructure of coating E. Loose particles can be seen on the coating surface.*

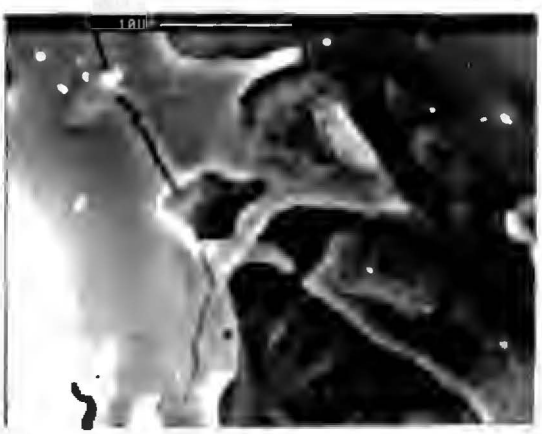

***Figure 4.19:** SEM micrograph of coating E showing how the powder has only partially melted.*

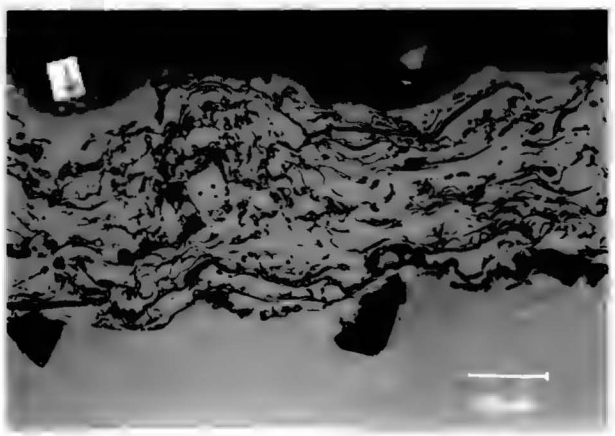

***Figure 4.20:** Optical micrograph showing the microstructure of coating F. Again loose particles are observed on the coating surface.*

The micrographs show the variation of coating thickness and porosity content for the eight as received coating materials. The measured thickness ranged from 228 μm for coating E to approximately 353 μm for coating F. The porosity content varied from 5 % for coatings C and E to approximately 22 % for coating H. The coating-substrate bond is also shown. The adherence between the coating and the substrate was found to range from 50 % for coating B to 90 % for coating A.

4.4. Surface roughness testing

The surface roughness was measured for both the coatings and the steel substrate, using a Taylor-Hobson Surtronic 3P stylus profilometer as discussed in Section 3.7. The surface roughness, Ra of the as received coatings was found to vary across the coating surface and also between the different coatings. For all the coatings the surface roughness was found to decrease with increasing amount of erosion, until a near constant value was reached. The opposite trend was observed for the steel specimen. These trends are shown for coating A and the boiler steel in Figure 4.21.

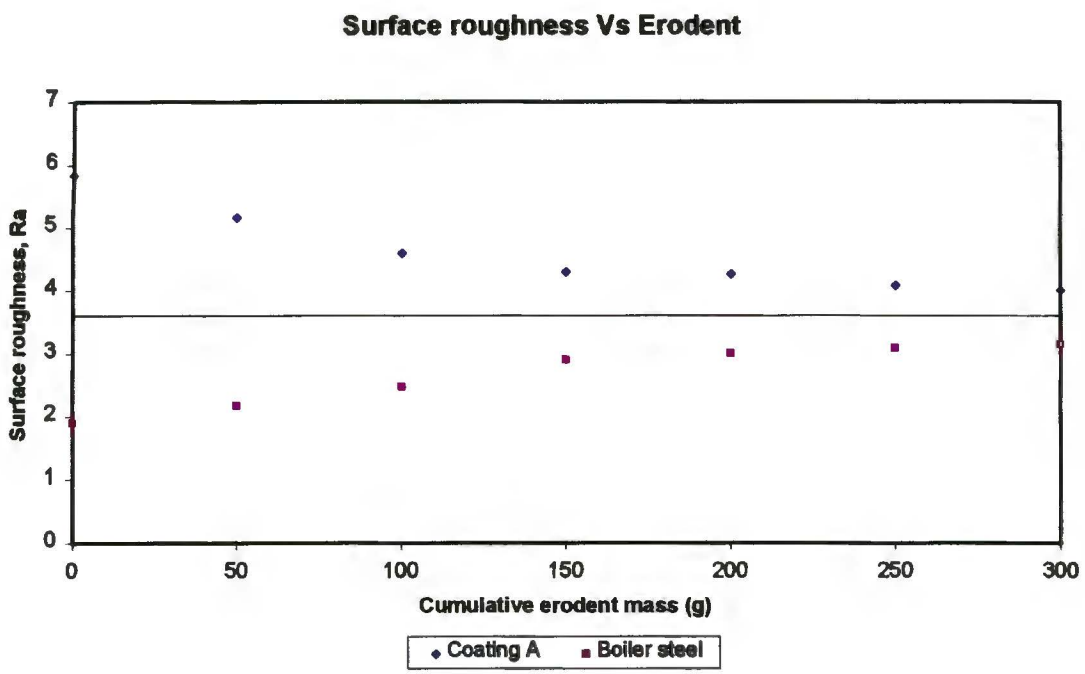

Figure 4.21: *Graph comparing the effect of surface roughness on the steel and coating A after erosion testing.*

It is interesting to note that the surface roughness of coating A and the boiler steel tended toward a similar Ra value of 3.5 μm during the course of erosion testing.

4.4.1. Summary of roughness test results

Coating	Surface Roughness, R_a								
	Test1	Test2	Test3	Test4	Test5	Test6	Test7	Test8	Test9
A	5.83	5.16	4.59	4.29	4.26	4.08	4.00	3.97	
B	7.69	4.58	4.01	3.49	3.33	3.22	3.10	3.05	
C	4.25	3.26	3.13	3.07	2.97	2.82	2.73		
D	17.9	15.4	11.9	10.7	10.6	10.3	9.7		
E	12.6	8.5	7.8	7.77	6.26	6.22			
F	18.41	15.17	14.03	12.7	11.73	10.46			
G	15.45	11.39	9.53	9.07	8.92	8.43			
H	21.65	19.47	17.77	16.17	15.67	15.4	14.64	13.72	13.6
K	7.14	6.40	5.56	4.14	3.99	3.93	3.87		
L	18.51	13.34	11.63	9.71	9.67	9.64			
Steel	1.9	2.17	2.47	2.89	3.00	3.08	3.14		

***Table 7:** The table gives the surface roughness of the coatings and the boiler steel during the course of erosion testing. Test1 represents the initial surface roughness before any erosion testing.*

4.5. Hardness testing

A Matsuzawa microhardness tester was used to carry out hardness tests using a load of 50 gf as described in the Section 3.7. The hardness varied across the coating surface. The hardness was taken as the average of five measurements. The results of these hardness tests are presented in Table 8. It was found that the hardness of the coatings varied between 545 HV for coating H and 723 HV for coating A. The harder coatings A and B contained 88 % tungsten carbide in their microstructures as shown in Table 1, Section 3.1.1. The boiler steel was found to be much softer than all of the coatings. The hardness obtained was only 211 HV. Thus the hardest coating A is almost 3.5 times harder than the boiler steel.

There is large scatter in hardness values for the coatings, which did not perform well, e.g. the measured hardness values for coating H ranged from 525 – 560 HV. More consistent hardness values were measured for the better quality coatings and the boiler steel, e.g. the hardness values obtained for the steel varied between 207 and 214 HV

Coating	*Average Vickers Hardness (HV)*	*Variance obtained in hardness values*
A	*723*	*715 - 730*
B	*697*	*700 - 712*
C	*709*	*690 - 710*
D	*682*	*675 - 685*
E	*642*	*660 - 685*
F	*679*	*625 - 657*
G	*585*	*565 -590*
H	*545*	*525 - 560*
K	*715*	*712 - 719*
L	*655*	*640 - 677*
Steel	*211*	*207 - 214*

Table 8: The table shows the hardness of the as received coatings and boiler steel.

4.6. Coating thickness

The thicknesses of the coatings are presented in Table 9. The thickness of the coatings ranges between 228 μm for coating F and 353 μm for coating E. All the coatings show a large range in the measured coating thicknesses. This is also an indication of the surface roughness of the coatings.

Coating	*Average Thickness (μm)*	*Variance obtained for thickness (μm)*
A	*298*	*280 - 312*
B	*338*	*333 - 357*
C	*323*	*313 - 350*
D	*282*	*260 - 308*
E	*353*	*330 - 375*
F	*228*	*190 - 240*
G	*275*	*210 - 290*
K	*243*	*237 - 248*
L	*251*	*247 - 255*
H	*303*	*290 - 320*

***Table 9:** The table gives the thicknesses of the eight as received coatings.*

4.7. Porosity

The porosity content of the coatings was determined semi-quantitatively by lineal analysis and the results are shown in Table 10. The porosity content was also determined using image analysis techniques. These processes of lineal analysis and image analysis were described in the experimental procedures, Section 3.9. It was found that the porosity content ranged from 5 % for coatings B and F to 22 % for coating H. This means that almost one quarter of coating H consists of porous regions.

The variance in values obtained for porosity measurements using lineal analysis indicate that the pores within the coatings were not uniformly distributed. The results obtained using lineal analysis and the more reliable image analysis technique compare very well. The difference in the measured values for these two techniques ranged from 1.4 % for coating G to 8.6 % for coating H.

Coating	*Ave. % Porosity (Lineal analysis)*	*Variance in values obtained (%)*	*% Porosity (Image analysis)*
A	*6*	*5 - 8*	*5.4*
B	*5*	*2 – 7*	*5.9*
C	*7*	*5 - 8*	*5.3*
D	*10*	*7 - 13*	*11.1*
E	*13*	*11 - 17*	*5.5*
F	*5*	*2 - 7*	*13.1*
G	*14*	*10 - 17*	*13.8*
K	*6*	*4 - 8*	*6.3*
L	*11*	*9 - 14*	*12.1*
H	*22*	*14 - 29*	*20.9*

Table 10: The table shows the porosity content the eight as received coatings.

Chapter 5

Discussion

In the present work a series of eight thermally sprayed metallic coatings have been evaluated for their ~~solid~~ particle erosion resistance at 400°C and compared to the erosion resistance of boiler tube steel. The influence of erodent velocity, surface profile, hardness and porosity on these erosion rates has also been determined. A discussion of these results follows.

5.1. Erosion behaviour

The results of erosion testing on the as received coatings show that the erosion rate is not consistent over the period of testing. Initially, the rate of material loss from the surface is high which decreases with the time of testing until a steady state erosion rate is achieved. This transient period, before steady state conditions are established, was found to be similar for all the coatings. However, in the case of boiler steel no transient period was observed and a constant rate of erosion was observed throughout testing.

The various processes of thermal spraying are generally based on methods in which a metallic or non metallic wire or powder is melted and the fused particles are projected unto a prepared surface in order to build up an adherent layer of suitable thickness. All of the coatings tested in this work were applied manually using a plasma spraying technique and all exhibited inconsistencies both in the quality of the coating and in the surface profile and characteristics. The surfaces of the coatings were found to not only vary in their surface roughness values, which ranged from approximately 4 μm to 22 μm Ra, but were oxidised and exhibited defects in the form of semi fused powder particles.

Metallographic investigation, using the scanning electron microscope (SEM) also revealed the formation of cracks on the uneroded surface of the coatings as shown in Figure 5.1. Figure 5.1 also shows how the powder used for the coating has only partially melted. Thus, in the initial stages of erosion, any partially fused particles on the surface are easily removed,

together with brittle oxide layers and the prominent surface peaks of fused material. This results in the recording of high erosion rates. With increasing erosion, the surface profile continuously changes, eventually leading to the establishment of an approximately constant value of roughness Ra as shown in Section 4.4. Simultaneously, the measured erosion rate continuously decreases until the surface profile stabilises and steady state erosion conditions ensue.

Figure 5.1: *SEM micrograph depicting the formation of cracks and unmelted regions on the uneroded surface of coating E.*

No transient period of high erosion rates was observed during the testing of the boiler steel which had a smoother more consistent surface compared to those of the coatings. Consistent erosion rates were found throughout the period of testing and a stable surface roughness profile was quickly established. Similar results were also obtained for coatings where the surfaces were initially ground to remove the inconsistencies and to achieve a surface roughness Ra of approximately 2.10 μm similar to the as received boiler steel surface. The erosion rates were found to be steady throughout the test period for these ground surfaces confirming that easy erosion of surface inconsistencies for the as received coated samples were responsible for the high initial erosion rates. Furthermore Figure 5.2 illustrates that the erosion rates measured on the ground samples were similar to those measured during steady state erosion for similar as received coatings. It is thus important in the measurements of erosion rates to establish consistent conditions in order for meaningful comparisons to be made.

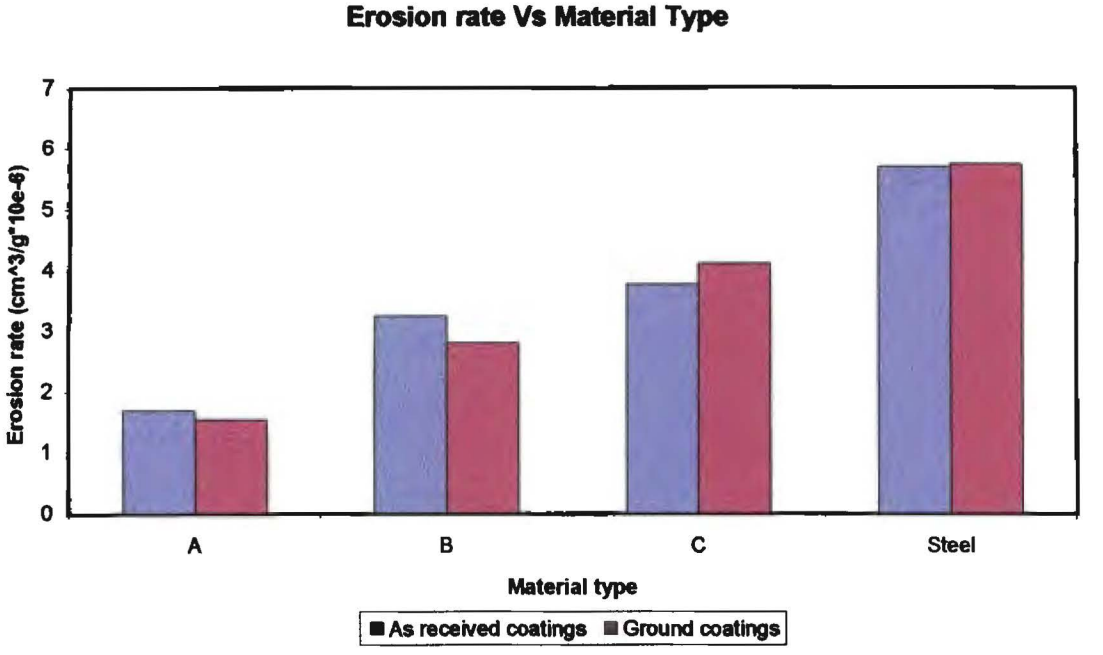

Figure 5.2: *Histogram comparing the erosion rates of coatings and the boiler steel specimen before and after grinding.*

Experiments carried out on actual boiler tubes, which had been coated, showed similar behavioural erosion patterns to those of the as received coated flat specimens of high initial erosion followed by steady state conditions. In all cases, however, the recorded erosion rates were lower for the coated tubes compared to similar flat specimens, which is shown in Figure 5.3. This can be explained by the fact that erosion rates for all materials are known to vary with the attack angle. Ductile materials exhibit the highest erosion rates between 30° and 40°, whilst brittle materials have the least erosion resistance at an attack angle of 90° [6, 11, 24].

In this work the attack angle chosen for the flat specimens was 40° to achieve high erosion rates. Thus it is to be expected that a variable attack angle between 0° and 90° for the coated tubes and the boiler steel would yield lower erosion rates for these "ductile" coatings and steel. For purely ductile erosion, any change in attack angle from 40° will lead to a lowering of erosion rates. However the maximum in the erosion rate curve with attack angle is likely to be above 40° for the coatings, in which case any decrease in the overall rate of erosion for

these cylindrical specimens is likely to be smaller. The reduction in erosion rate for the boiler steel is approximately 100 % but varied between 15 % and 59 % for the coatings.

This variability in the reduction of erosion rates for similar coatings applied to tubes and those deposited on flat specimens is also believed to be partly due to the difficulty in achieving consistent quality of similar coatings which were applied at different times. The variability in the structure and composition of the individual coatings which gives rise to different mechanical properties and associated modes of material removal are discussed later in this chapter.

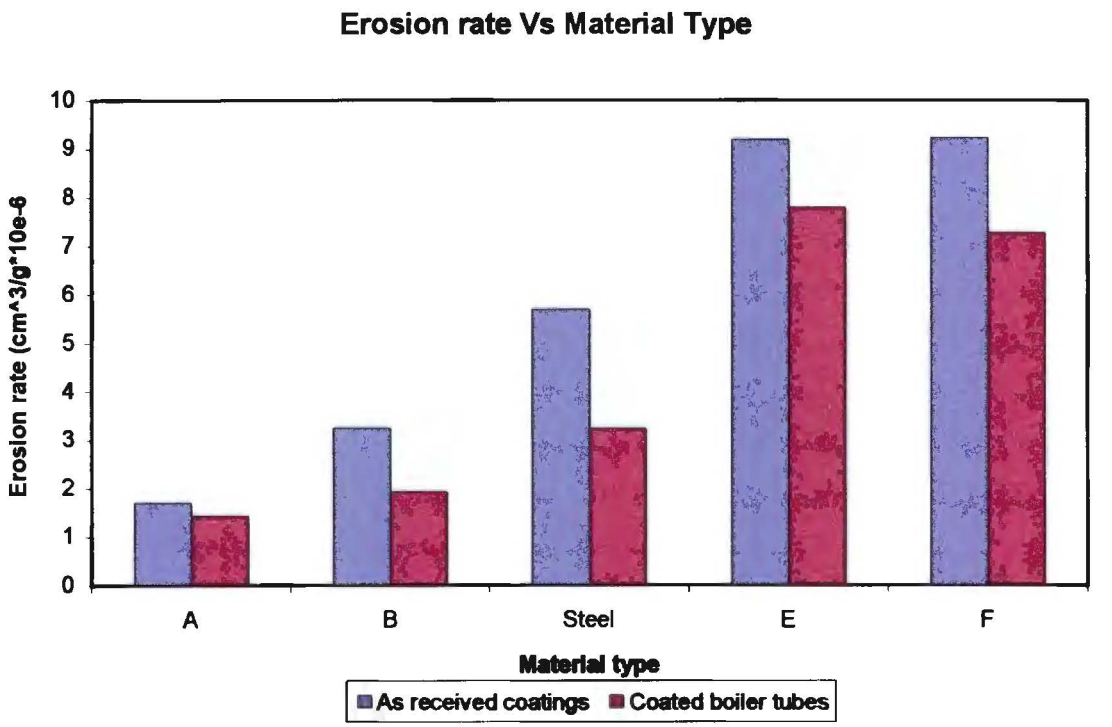

Figure 5.3: *Histogram comparing the erosion rates of the as received coatings and the as received coated boiler tubes with the standard steel specimens.*

5.2. Effect of microstructure

An explanation for the large differences in the erosive wear performance of the coatings and the steel can be found based on the microstructure and mode of material removal during erosion. The microstructure of these coatings vary and are not consistent due to the method of application in which molten or semi-molten particles are sprayed onto a 'cold' steel surface. In practice this is also carried out in situ on the boiler tubes. This process results in inhomogeneous, non-equilibrium structures, which contain in addition to partially fused particles different phases, oxides and porosity.

Generally it was found that the coatings based on hard carbides such as tungsten carbide exhibited a finer more homogenous structure and lower erosion rates than those based on metallic elements alone. This is in agreements with Olsson et al [68] who found that a fine grain size, low porosity and a good coating-substrate adhesion promote better wear resistance.

5.3. The effect of porosity

Figures 5.4 demonstrates the extent to which porosity can occur in these coatings, the percentages of which were listed in Table 10, Section 4.7 for all the coatings.

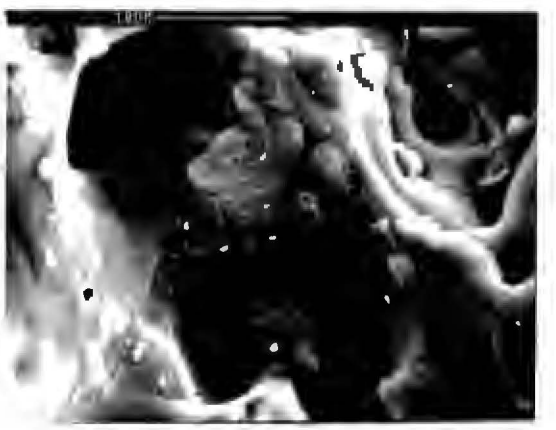

***Figure 5.4:** SEM micrograph showing pores in the microstructure of coating E.*

The influence of porosity on erosion rates shows a strong correlation between increasing erosion rate and increasing porosity as shown in Figure 5.5. This is in agreement with earlier work of Olsen et al [68]. It should be noted however that the measurement of porosity is prone to large scatter due to the method of coating application which results in a great deal of variation in the microstructure.

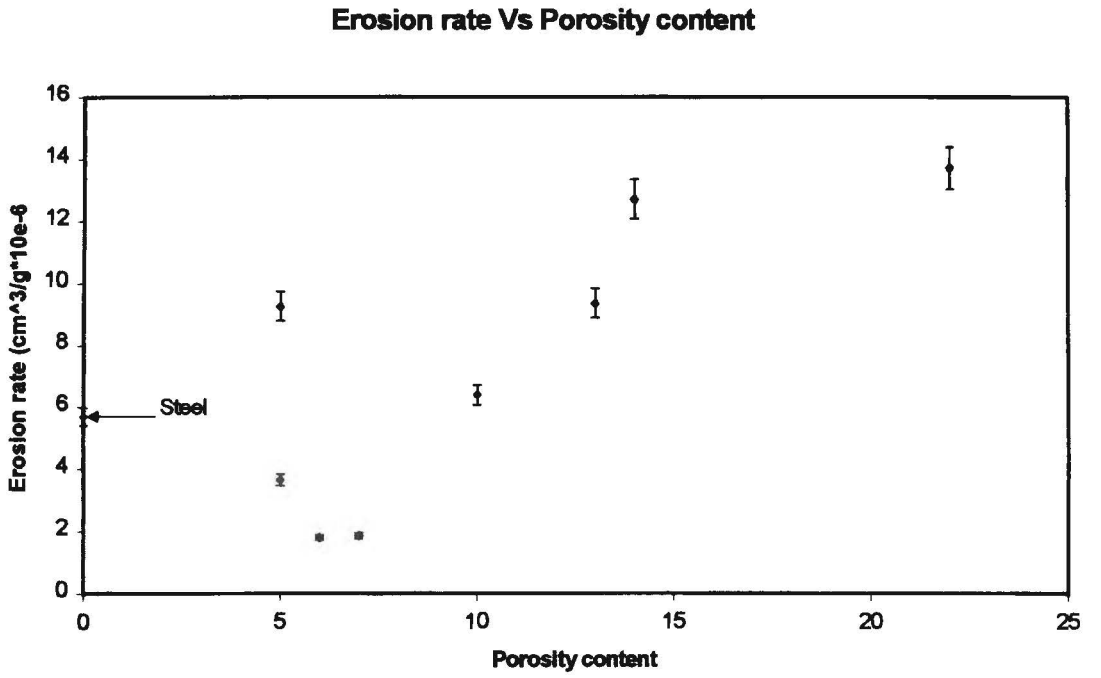

***Figure 5.5:** Relationship between the porosity content of the eight as received coatings and the erosion rate.*

The error bars give an indication of the uncertainty in the value obtained. The error is relatively small ± 5 % for the better quality coatings A, B and C, which performed better than the boiler steel. The porosity in these coatings was found to be finely distributed in the microstructure. However the error is much larger ± 12 % for the coatings that performed worse than the boiler steel. The porosity was found to be coarse and not uniformly distributed in the microstructure, which is also an indication of the quality of the coatings.

Clearly the amount, size and distribution of pores within the coatings all have an influence on the ease with which material can be removed. It would seem very important that if porosity cannot be avoided then fine well dispersed pores will minimise the effect of these defects on

the erosion rates. As indicated on the graph, the porosity content of steel was taken to be zero. It is important to note though that this does not imply that the erosion rate will be zero.

5.4. The effect of hardness

The hardness for the coatings ranged from 545 HV for coating H to 723 HV for coating A. Not surprisingly, the coatings with tungsten carbide (WC) in their microstructure, A and C, were found to be the hardest. Figure 5.6 shows that the erosion rates of the coatings generally decreases with increasing coating hardness. Hogmark and Hedenqvist [67] also found that increasing erosion rates can be related to decreasing coating hardness when they examined the tribological behaviour of thin, hard physically deposited (PVD) coatings such as titanium-nitride (TiN), which is in agreement with this work. Figure 5.6 also shows that the much softer boiler tube steel is outperformed by only three of the comparatively much harder coatings. The remaining coatings, despite their higher hardness, performed worse than the boiler steel substrate. Therefore the use of the hardness value alone is not sufficient to draw a conclusion about the erosion rate of the coatings or the boiler steel.

Davis et al [70] also stated that hardness is not a dominating factor, but rather that the apparent porosity of the coatings has a greater influence on erosion rates. This is also in agreement with Burnett and Rickerby [71] and Chiu and Liou [72]. There is evidence in the literature that porosity actually lowers the hardness [65]. Such results have been found many times previously in the determination of wear under different conditions. Other properties of the coatings and erodent play a significant role in the determination of erosion behaviour such as porosity as discussed earlier.

5.5. The effect of oxides

An attempt was made to measure the amount of oxide in these coatings using image analysis techniques but without success due to the difficulty of distinguishing clearly between the oxide, porosity and some phases in the coating. Qualitatively, those coatings in which the oxides were small and well dispersed gave erosion rates lower than the other coatings. The porosity and oxides were finely and uniformly distributed in the tungsten carbide dominated

microstructure of coatings A and B which were subsequently found to have lower erosion rates compared to the rest of the coatings.

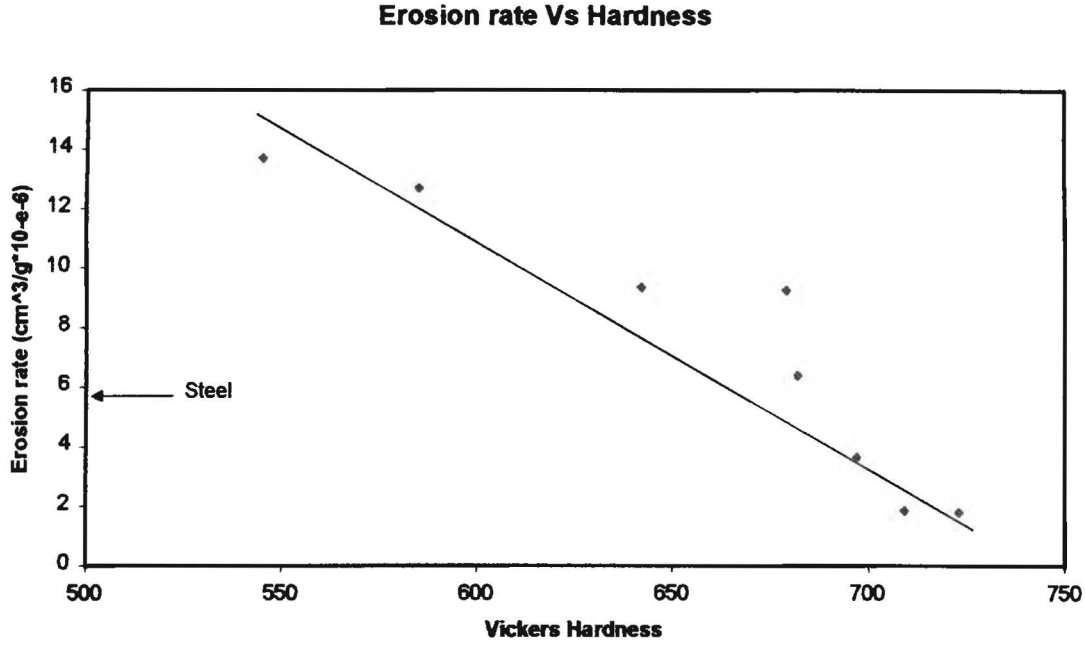

***Figure 5.6:** The erosion rate clearly decreases with increasing coating hardness for the eight as received coatings.*

5.6. The effect of erodent velocity

It found in this work that the erosion rate increased with increasing impact erodent velocity for the plasma sprayed coating E, which has been found to be typical of all materials [4]. A power law curve was obtained with a velocity exponent, n of 1.97. This is expected since

$$E_k = 0.5mv^2$$

where E_k = kinetic energy, m = mass and v = velocity.

This means that the kinetic energy is directly related to the erodent impact velocity to the power of two. These findings are in agreement with Tabakoff et al [4] who performed similar tests on a range of coating materials and ductile stainless steel. They obtained velocity exponents greater than 2 for coatings applied via the detonation gun technique (See section 2.3.2.3), while the values obtained for the stainless steel varied between 1.37 and

velocity exponent obtained for the plasma sprayed coating was found to be less than 2. Tabakoff and co-workers concluded that the different values obtained at the same test conditions were an indication of the material properties effect on the erosion behaviour. They concluded that the strong effect of velocity on the erosion rate is manifested by the high value obtained for the velocity exponent, n.

5.7. Mechanisms of material removal

In general the manner in which material is removed from the steel and coating surfaces showed three different modes which appear to be related to the structure of the coatings.

In the case of the boiler steel it was found that a typical ductile erosive wear mechanism operates. Single erosive impact strikes on a polished steel surface show the typical features associated with a ductile erosive wear process consisting of surface deformation and ploughing and the appearance of protrusions or shear lips. The loss of material occurs through the cutting action of the erodent producing debris and the overall loss of highly strained projections from subsequent impacts of erodent particles (Figure 5.7). These findings are in agreement with Bellman and Levy [9] who reported that the basic erosion mechanism in single-phase materials is considered to be a combination of micromachining, ploughing processes and damage accumulating processes.

***Figure 5.7:** SEM micrograph of a single solid particle impact event on a polished boiler steel specimen.*

Figure 5.8 shows the erosive wear damage on the surface of the boiler steel sample after blasting with SiO_2 erodent for 300 minutes. Extensive plastic deformation is observed on the steel surface. Material is displaced through cuts and the formation of craters and lips. This is similar to Levy et al [10] who found that after many impacts the surface becomes covered with displaced deformed material, which form platelets. The platelets display ductile cracks around the edges and are removed by subsequent particle impacts.

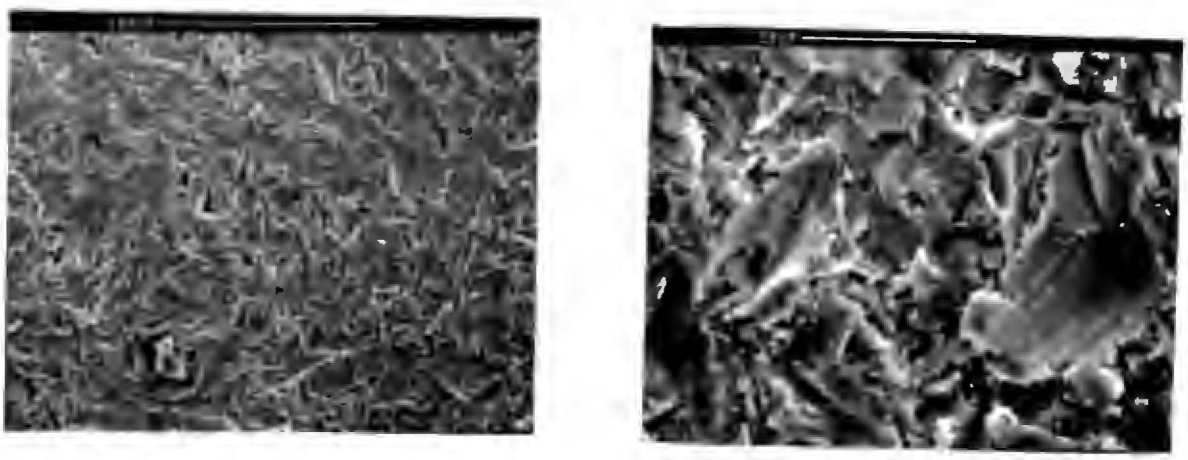

***Figure 5.8:** SEM micrographs showing the plastic deformation on the surface of the steel specimen after erosion for 300 minutes.*

Similar deformation characteristics can also be observed when single impact strikes are viewed on a polished coating surface. In addition, however, cracking and chipping of segments of the coatings were also observed (Figure 5.9). These cracks appeared to be associated with areas where there is a sharp transition in the structure and properties of the coatings such as at phase and oxide interfaces often associated with porosity in the structure. Such chipping leads to the loss of larger masses of material than simple ductile erosion and thus gives rise to higher erosion rates. Thus it is to be expected that as the microstructure becomes coarser and or the amount of porosity and entrapped oxides increases, the erosion rates increase, which was generally found in this work.

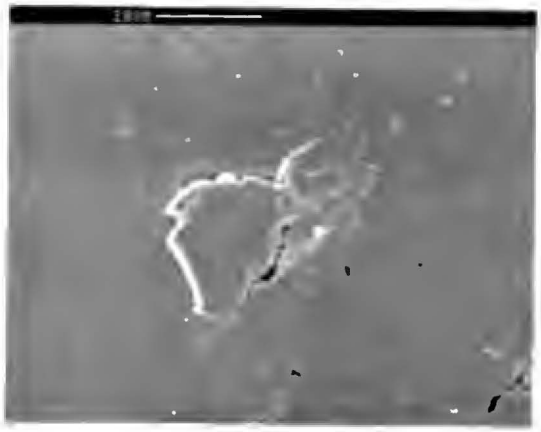

Figure 5.9: *SEM micrograph of a single impact event on the surface of a polished coating.*

Material removal from the finer more homogeneous carbide coatings show that surface deformation is much less than that for the ductile steel. It would appear that repeated impacts eventually lead to work hardening and surface cracking and the ultimate loss of material.

Figure 5.10 shows the damage on the surface of coating A after erosion for 300 minutes in the high temperature erosion apparatus. Coating A (Figure 5.10) with predominantly tungsten carbide (WC) in its microstructure shows some plastic deformation and smearing of material across the surface, together with surface cracking. There is no evidence that the loss of the ductile binder phase occurs prior to tungsten carbide (WC) loss, but rather that fracture eventually leads to the loss of volumes of material. However it mainly shows that material is simply broken off the surface resulting in material loss.

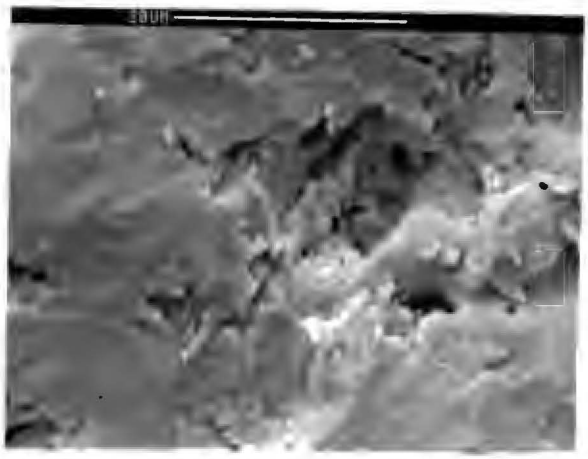

Figure 5.10: *SEM micrograph depicting an impact site on the surface of coating A. While some plastic deformation is observed material is mainly broken off the surface.*

In summary, the mode of material removal is closely related to the microstructure of the coatings and the boiler steel. Whilst the boiler steel show typical features associated with a ductile erosive wear process, the coatings based on hard carbides show that the surface deformation is much less and that chunks of material are broken off the surface. It was found that in those coatings based on metallic elements alone, material was also removed via a chipping process at the weak interfaces in the microstructure in addition to any ductile erosive wear mechanism.

Chapter 6

Conclusions

- The erosion resistance of the eight coatings examined was found to vary by many orders of magnitude. Only four of these coatings, containing hard carbides in a ductile binder exhibited lower erosion rates than the boiler steel.

- A strong correlation was found between the porosity of the coatings and the erosion resistance; higher porosity leading to higher erosion rates.

- An exponential law was found relating erosion resistance to erodent velocity. The velocity exponent was determined to be 1.97.

- The quality of the coatings was found to vary significantly. Those coatings with fine microstructures in which defects were small and well dispersed had the best erosion resistance.

References

1. **E. Lang** (Ed.), *Coatings for High Temperature Applications,* A Publication of the CEC High Temperature Materials Information Centre, Petten (n.H.), Netherlands, 1984.

2. **I. M. Hutchings,** *Tribology: Friction and Wear of Engineering Materials,* **E. Arnold,** Wear by hard particles, 1986, 133.

3. **A. V. Levy, M. Aghazadeh and G. Hickey,** *The Effect of Test Variables on the Platelet Mechanism of Erosion,* Rep. LBL-17835, 1984 (Lawrence Berkeley Laboratory, University of California, Berkeley, CA, USA).

4. **W. Tabakoff, M. Metwally and A. Hamed,** *High Temperature Coatings for Protection Against Turbine Deterioration,* Journal of Engineering for Gas Turbines and Power, 117, January 1995, 146.

5. **M. T. Benchaita, P. Griffith and E. Rabinowicz,** *Erosion of Metallic Plate by Particles Entrained in a Liquid Jet,* Journal of Engineering for Industry, 105, August 1983, 215.

6. **G. Sundararajan,** *The Depth of Plastic Deformation Beneath Eroded Surfaces: The Influence of Impact Angle and Velocity, Particle Shape and Material Properties,* Wear 149, 1991, 129.

7. **M. B. Suckling and C. Allen,** *Ash Erosivity Differences Between Coal Fired Power Generating Units,* Conf. Proc., "Tribology in Power Generation", Pretoria, 27-29 September 1994.

8. **A. V. Levy and P. Chik,** *The Effects of Erodent Composition and Shape on the Erosion of Steel,* Wear 89 (2), 1986, 151.

10. **A. V. Levy, R. Bellman and J. Maasberg,** *Properties and Performance of Materials in the Coal Gasification Environment,* ASM, New York 1981 (also as Rep. LBL-12023, Lawrence Berkeley Laboratory, University of California, Berkeley, CA, USA).

11. **A. V. Levy,** *The Platelet Mechanism of Erosion of Ductile Metals,* Rep. LBL-15240, 1982, 1984 (Lawrence Berkeley Laboratory, University of California, Berkeley, CA, USA).

12. **I. M. Hutchings,** *Proc. Corrosion-Erosion of Coal Conversion Systems,* Materials Conf., 1979, NACE, Houston, TX, 393.

13. **R. Bellman, A. V. Levy** in **S. K. Rhee, A. W. Ruff and K. C. Ludema** (Eds), Proc. Int. Conf. On Wear of Materials, San Francisco, CA, March 30-April 1, 1981, ASME, New York, 1981, 564.

14. **P. Shewmon,** *Particle Size Threshold in the Erosion of Metals,* Wear 68, 1981, 253.

15. **R. A. Doyle and A. Ball,** *On the Thermomechanical Effects During Solid Particle Erosion,* Wear 151, 1991, 87.

16. **L. K. Ives and A. W. Ruff,** *Transmission and Scanning Electron Microscopy Studies of Deformation at Erosion Impact Sites,* Wear 46, 1978, 149.

17. **T. H. Kosel, A. P. L. Turner and R. O. Scattergood** in **K. Natesan** (Ed), *Corrosion-Erosion Behaviour of Materials,* AIME, New York, 1980, 146.

18. **Y. G. Wey, J. Moteff and L. K. Ives** in **K. C. Ludema** (Ed), Proc. Int. Conf. On Wear of Materials, Reston, VA, April 11-14, 1983, ASME, New York, 1983, 354.

19. **R. Brown, E. J. Jun and J. W. Eddington,** in **S. K. Rhee, A. W. Ruff and K. C. Ludema** (Eds), Proc. Int. Conf. On Wear of Materials, San Francisco, CA, March 30-April 1, 1981, ASME, New York, 1981, 583.

20. **A. K. Cousins and I. M. Hutchings,** in **J. E. Field and N. S. Corney** (Eds), Proc 6th Int. Conf. On Erosion by Liquid and Solid Impact, Cambridge, September 5 – 8, 1983, Cavendish Laboratory, Cambridge 1983, Paper 41.

21. **M. M. Stack, F. H. Stott and G. C. Wood,** *Review of Mechanisms of Erosion-Corrosion of Alloys at Elevated Temperatures,* Wear 162-164, 1993, 706.

22. **A. W. Ruff and S. M. Weiderhorn,** *Quantitative Methods in Wear Debris Analysis,* Treatise Materials Science Technology, 16, 1979.

23. **R. O. Scattergood and J. L. Routbort,** *Velocity Exponent in Solid Particle Erosion of Silicon,* Journal of American Ceramic Society, 66, 1983, C-184

24. **S. Wada and N. Watanabe,** *Solid Particle Erosion of Brittle Materials. The Interaction of Materials Properties and that of Impingement Particle on Erosive Wear Mechanisms,* Yogyo-Kyokai-Shi, 95 (6), 1987, 573.

25. **S. Wada, N. Watanabe and T. Tani,** *Solid Particle Erosion of Brittle Materials. The Effect of Impingement Angle,* Journal of Ceramic Society, Japan International Edition, 96, 1988, 737.

26. **A. G. Evans, M. E. Gulden and M. E. Rosenblatt,** *The Effect of Impacts on Erosion of Polycrystalline MgF_2 in the Elastic-Plastic Response Regime,* Proc. Roy. Soc, A361, 1978, 343.

27. **S. M. Wiederhorn and B. R. Lawn,** *Strength Degradation of Glass Impacted with Sharp Particles,* Journal of American Ceramic Society, 62, 1979, 66.

28. **B. R. Lawn and R. Wilshaw,** *Review Indentation Fracture: Principles and Applications,* Journal of Material Science, 10, 1975, 1049.

29. Idem. *"Fracture of Brittle Solids",* Cambridge Press, 1975.

30. **D. B. Marshall,** *"Nitrogen Ceramics"* **F. L. Riley** (Ed.), (Martinus Nijhoff, The Hague, 1983), 635.

31. **B. R. Lawn, B. J. Hockey and H. Richter,** *Indentation Analysis: Applications in the Strength and Wear of Brittle Materials,* Journal of Microscopy, 130, 1983, 295.

32. **J. E. Ritter, P. Strzepa and K. Jakus,** *Erosion and Strength Degradation in Soda-lime Glass,* Phys Chem. Glasses 25, 1984, 159.

33. **C. E. Smeltzer, M. E. Gulden and W. A. Compton,** *Mechanisms of Metal Removal by Impacting Dust Particles,* Journal of Basic Engineering, 1970, 92, 639.

34. **E. Raask,** *Erosion Wear in Coal Utilisation,* Hemisphere publishing corp., 1988, Distributed by Springer Verlag.

35. **F. H. Stott, S. W. Green and G. C. Wood,** *The Influence of Temperature on the Erosion Oxidation of Steels in a Fluidised-bed Environment,* Journal of Materials Science and Engineering, A121 (2), 1989, 611.

36. **V. K. Sethi and R. G. Corey,** Proc. 7th Int. Conf. on Erosion by Liquid and Solid Impact, Cavendish Laboratory, University of Cambridge, Cambridge, 1987, Paper 73.

37. **A. J. Ninham, I. M. Hutchings and A. J. Little,** *Erosion-Oxidation of Austenitic and Ferritic Alloys,* Proc. Conf. Corrosion, 1989, NACE, Houston TX, 1989, Paper 554.

38. **D. H. Hall and S. R. J. Saunders,** in **E. Bachelet** (Ed), Proc. High Temperature Materials for Power Engineering, 1, Kluwer, Liege, 1990, 157.

39. **A. V. Levy,** *The Erosion of Metal Alloys and Their Scales,* Proc NACE Conf. on Corrosion-Erosion-Wear of Materials in Emerging Fossil Energy Systems, Berkeley, CA, January 1982, National Association of Corrosion Engineers, Houston, Texas, 1982, 298.

40. **M. Emiliani and R. Brown,** *Erosion of Ti-6Al-4V by Spherical Silica particles of 90° Impact Angle*, Proc. 6th Int. Conf. on Erosion by Solid and Liquid Impact, Cambridge University, Cambridge, Cambs., September 1983, University of Cambridge, Cambridge, Cambs.

41. **R. R. Dils and P. S. Follansbee,** *Dynamic Oxidation and Corrosion in Power Generating Units,* Corrosion, 33 (11), Nov. 1977, 385.

42. **J. V. Cathcat and R. E. Pawel,** *The Mechanical Behaviour of Oxide Scales*, Conf. Proc.: Corrosion-Erosion of Coal Conversion System Materials, 24-26 January 1979, Berkeley, California.

43. **M. M. Stack, F. H. Stott and G. C. Wood,** *Erosion-Corrosion of Pre-oxidised Incology 800H in Fluidised Bed Environments: Effects of Temperature, Velocity and Exposure Time*, Materials Science and Technology, 7 December 1991, 1128.

44. **A. J. Ninham, I. M. Hutchings and J. A. Little,** *Erosion-Oxidation of Austenitic and Ferritic Alloys*, Corrosion Magazine, 4 - 6 April 1990, 296.

45. **B. Wang, G. Geng and A. V. Levy,** *Erosion and Corrosion of Cooled 1018 Steel*, Wear 161, 1993, 41.

46. **J. A. Maasberg and A. V. Levy,** *Erosion of Elevated Temperature Corrosion Scales on Metals*, Wear 73, 1981, 355.

47. **G. Zambelli and A. V.Levy,** *Erosion of Oxide Scales on Metal Substrates*, Conf. Proc.: Corrosion-Erosion of Coal Conversion System Materials, 24 - 26 January 1979, Berkeley California.

48. **A. R. Nicoll,** *A survey of Methods Used for the Performance Evaluation of High Temperature Coatings,* **in E. Lang** (Ed.), Coatings for High Temperature Applications, A

Publication of the CEC High Temperature Materials Information Centre, Petten (n.H.), Netherlands, 1984, 269.

49. **S. Agarwal and M. A. H. Howes,** *Erosion-Corrosion of Materials in High Temperature Environments*, Proc. AIME Conf. on High Temperature Corrosion in Energy Systems, Detroit, MI, September 1984, Metallurgical Society of AIME, Warrendale, PA, 1985.

50. **V. Nagarajan, I. G. Wright,** *Influence of Oxide Scales on High Temperature Corrosion-Erosion Behaviour of Alloys*, Proc. NACE Conf. on High Temperature Corrosion, San Diego, CA, March 1981, NACE, Houston, TX, 1983, 398.

51. **T. Tiainen,** *Simulation of the Erosion and Corrosion of Materials in Fluidised Bed Combustors*, Proc. AIME Conf. on High Temperature Corrosion in Energy Systems, MI, September 1984, Metallurgical Society of AIME, Warrendale, PA, 1985.

52. **A. V. Levy,** *The Origin of Solid Particle Erosion,* Corrosion-Erosion-Wear of Materials at Elevated Temperatures, 1986, 387.

53. **I. G. Wright, V. K. Sethi and V. Nagarajan,** *An Approach to Describing the Simultaneous Erosion and High Temperature Oxidation of Alloys*, Transactions of the ASME, 113, October 1991, 616.

54. **F. W. Wood,** *Erosion by Solid Particle Impacts: A Testing Update*, Journal of Testing and Evaluation, JTEVA, 14 (1), January 1986, 23.

55. **J. A. Laitone,** *Aerodynamic Effects in the Erosion Process*, Wear 56, 1979, 239.

56. **S. Bahadur and R Badruddin,** *Erodent Particle Characterisation and the Effect of Particle Size and Shape on Erosion*, Wear 138, 1990, 189.

57. **Wada** in **S. Srinivasan and R. O. Scattergood**, *Effect of Erodent Hardness on Erosion of Brittle Materials*, Wear 128, 1988, 139.

58. **R. A. Vaughn and A. Ball,** *Erosion Processes for Hard Materials Subjected to Impact by Different Erodents,* Journal of Hard Materials 2, 1991, 257.

59. **R. A. Vaughn,** *The Effects of Hardness, Toughness, Microstructure and Thermomechanical Heating on the Erosion of Ceramic and Ultrahard Materials,* MSc Thesis, University of Cape Town, 1991.

60. **H.. D. Steffens,** *Spray and Detonation Gun Technologies, Laser Assisted Techniques,* **in E. Lang** (Ed.), Coatings for High Temperature Applications, A Publication of the CEC High Temperature Materials Information Centre, Petten (n.H.), Netherlands, 1984, 121.

61. **K. T. Scott and R. Kingswell,** in **D. S. Rickerby and A. Matthews** (Eds), *Advanced Surface Coatings: A Handbook of Surface Engineering,* Chapman and Hall, New York, 217.

62. *Materials and Components in Fossil Energy Applications,* EPRI, No. 125, 1 December 1996, 7.

63. **A. P. Bennett and M. B. C. Quigley,** *The Spraying of Boiler Tubing in Power Stations,* Welding and Metal Fabrication, November 1990, 485.

64. **G. Wright and D. Haywood,** *Elevated Temperature Erosion of Selected Thermally Applied Coatings,* The South African Mechanical Engineer, 38(2), 1988, 157.

65. **H. D. Steffens, H. A. Crostack and J. Beczkowiak,** *Testing and Inspection of Coatings,* **in E. Lang** (Ed.), Coatings for High Temperature Applications, A Publication of the CEC High Temperature Materials Information Centre, Petten (n.H.), Netherlands, 1984, 193.

66. **V. Sedlacek,** *Metallic Surfaces, Films and Coatings,* Czech Technical University, Czechoslovakia, 1992.

67. **S. Hogmark and P. Hedenqvist,** *Tribological Characterisation of Thin, Hard Coatings,* Wear 179, 1994, 147.

68. **M. Olsen, P. Hedenqvist, B. Stridh and S. Soderberg,** *Solid Particle Erosion of Hard Chemically Vapour Deposited Coatings*, Surface Coatings and Technologies, 30, 1995, 1018.

69. **K. Holmberg and A. Matthews,** *Properties, Technologies and Applications in Surface Engineering*, Coatings Tribology, 1994.

70. **G. Davis, D. H. Boone and A. V. Levy,** *Erosion of Ceramic Thermal Barrier Coatings*, Wear 110 (2), 1986, 101.

71. **P. J. Burnett and D. S. Rickerby,** *The Wear and Erosion Resistance of Hard PVD Coatings*, Surface Coatings & Technology, 33, 1987, 191.

72. **C. C. Chiu and Y. Liou,** *Low Velocity Impact Damage in Brittle Coatings*, Journal of Materials Science, 30, 1995, 1018.

73. **R. O. Scattergood and J. L. Routbort,** *Transient and Synergistic Effects in Solid Particle Erosion of Silicon*, Journal of the American Ceramic Society, Vol. 64 (8), August 1981, C104.

74. **M. B. Suckling,** *Erosive Wear of Boiler Tube Steel*, PhD Thesis, University of Cape Town, 1997.

75. **T. R. Thomas** (Ed.), *Rough surfaces*, Longman, 1982.

APPENDIX A

Operating procedure of the HTER

What follows is a step-by-step procedure for operating the high temperature erosion rig (HTER). Refer also to Section 3.2 when reading the procedure.

Start up

- Open the valve at the main compressed air junction.
- Purge water from the filter for about 10 seconds.
- Adjust the pressure control valve to the desired pressure and thus the desired impact particle velocity.
- Switch both wall plugs to on.
- Switch eurotherm to on and set to 150°C.

Leave to warm up for 20 minutes if apparatus has been in continuous use, otherwise 40 minutes.

Computer and temperature measurement

- Switch computer on and at the DOS prompt type:
- cd martin
- c:>martin\cd card2
- c:>martin\card2\vistemp

The program will then ask how many thermocouple readings are to be taken. Reply 2 and press enter.

Setting up a test

- Run rig until the eurotherm reads 150°C on the analogue dial. Preheater is then at maximum operating temperature.
- The rig takes about 25 minutes to achieve maximum preheat.
- Close the brass tap on t-piece near the water valve.
- Open water valve fully.
- Check to see that the cooling system is operating properly by touching it briefly.

- Attach the specimen the specimen stage with the screw from the back of the stage.
- Ensure that the thermocouple is inserted into the side of the specimen.
- Ensure that the gasket is intact and in a good condition.
- Replace the coverplate and secure with wingnuts.

Using the gas flame

- Check that the valve at the burner neck is closed (perpendicular to the pipe).
- Open the valve on the gas bottle.
- Open the pressure control valve on the regulator until the supply reads approximately 30 kPa.
- Open valve at the burner neck and ignite the gas stream.
- Adjust the pressure control valve to the desired pressure.

For high particle velocities a high supply pressure is needed, meaning a high gas supply pressure. The system needs about 10 minutes to reach a steady temperature.

- Switch the power supply for the turntable on and check that it is rotating.
- Drop the measured amount of erodent through the supply hopper and start the stop watch.
- Stop the stop watch when all of the erodent has run out.

- Turn the gas pressure down to about 40 kPa and shut off the supply at the neck.
- Wait until specimen temperature drops to approximately 150°C before donning Kevlar gloves and removing the cover plate.
- Care should be taken as all surfaces of the HTER at this stage are in excess of 150°C.
- Allow the specimen to air cool before washing it in alcohol.
- Blow dry the specimen and proceed to weigh.

Shutdown

- Close the valve of the gas bottle.
- Purge the remaining gas from the line by opening the valve at the burner neck.
- Close the valve at the burner neck.
- Switch off the preheater in the reverse order to the start up, i.e
- Set the eurotherm to 50°C.

- Switch off the eurotherm.
- Switch off both the wall plugs.
- Close the water valve at the wall.
- Open the brass tap at the t junction near the water valve
- Leave the air running for about 45 minutes then switch off.

APPENDIX B

Summary of erosion test results on as received specimens

Table 4 summarises the mass loss measurements, time and temperature for each erosion test on the different coatings. It took on average 55 minutes to pass 50 g of erodent through the erodent feed hopper, while the temperature was maintained at about 400°C ± 10°C during the whole period of testing which extended for approximately six hours.

Coating	*Test*	*Mass loss (mg)*	*Time(min)*	*Temp (°C)*
A	*1*	*9.87*	*54:28sec*	*402*
A	*2*	*2.45*	*53:18sec*	*405.5*
A	*3*	*1.89*	*55:19sec*	*407*
A	*4*	*1.58*	*54:29sec*	*401*
A	*5*	*1.30*	*53:52sec*	*398*
A	*6*	*1.30*	*53:29sec*	*410*
A	*7*	*1.15*	*52:52sec*	*405*
B	*1*	*10.37*	*56:32sec*	*401*
B	*2*	*2.39*	*55:46sec*	*407.5*
B	*3*	*1.78*	*54:35sec*	*395*
B	*4*	*1.72*	*58:56sec*	*398*
B	*5*	*1.42*	*53:52sec*	*402.5*
B	*6*	*1.25*	*53:29sec*	*397*
B	*7*	*1.23*	*52:53sec*	*400.5*
C	*1*	*10.13*	*55:54*	*402*
C	*2*	*3.08*	*54:36*	*400.5*
C	*3*	*2.55*	*54:53*	*398*
C	*4*	*2.29*	*55:08*	*395*
C	*5*	*2.21*	*55:19*	*408*
C	*6*	*2.18*	*55:37*	*404*
D	*1*	*8.87*	*55:32sec*	*399*
D	*2*	*3.10*	*58:36sec*	*391*
D	*3*	*2.75*	*57:08sec*	*398*
D	*4*	*2.53*	*57:12sec*	*406*
D	*5*	*2.50*	*58:13sec*	*404.5*
D	*6*	*2.45*	*58:19sec*	*407*

Coating	*Test*	*Mass loss (mg)*	*Time (min)*	*Temp (°C)*
E	*1*	*14.02*	*58:51sec*	*406*
E	*2*	*4.82*	*59:36sec*	*408.5*
E	*3*	*4.63*	*56:29sec*	*410*
E	*4*	*3.67*	*59:30sec*	*404*
E	*5*	*3.59*	*58:11sec*	*407*
E	*6*	*3.58*	*55:11sec*	*408.5*
F	*1*	*14.10*	*54:23sec*	*400.5*
F	*2*	*4.30*	*55:57sec*	*408*
F	*3*	*3.90*	*54:02sec*	*410.5*
F	*4*	*3.70*	*53:54sec*	*414*
F	*5*	*3.60*	*53:54sec*	*403.5*
G	*1*	*17.21*	*57:23sec*	*399.5*
G	*2*	*5.89*	*54:00sec*	*395.5*
G	*3*	*4.60*	*55:06sec*	*401*
G	*4*	*4.60*	*53:21sec*	*404.5*
G	*5*	*4.60*	*53:26sec*	*405*
H	*1*	*30.57*	*59:30sec*	*401*
H	*2*	*8.24*	*58:27sec*	*397*
H	*3*	*5.93*	*57:58sec*	*395*
H	*4*	*5.56*	*58:30sec*	*403*
H	*5*	*5.07*	*57:17sec*	*407*
H	*6*	*4.73*	*54:34sec*	*409.5*
H	*7*	*4.40*	*54:51sec*	*405.5*
Steel	*1*	*2.41*	*54:37*	*404.5*
Steel	*2*	*2.28*	*54:07*	*400*
Steel	*3*	*2.19*	*55:18*	*397*
Steel	*4*	*2.14*	*53:54*	*398.5*
Steel	*5*	*2.11*	*54:34*	*402*

Table 11: *Summarising the mass loss measurements, the time and the temperature for the coatings and boiler steel.*

APPENDIX C

Surface roughness measurements

The surface roughness was measured using the stylus profilometer discussed in Section 3.7. The main parameters used are the peak to valley height, R_t, and the centre line average value, R_a. Also used is the root mean square value, R_s The average roughness, R_a, is the arithmetic mean deviation of the surface height from the mean line through the profile. Equal areas of the profile lie above and below this mean line, as shown below.

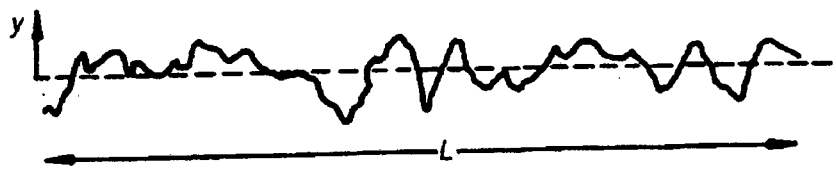

Therefore,

$$R_a = \frac{1}{L}\int_0^L |y(x)|\,dx$$

where y is the height of the surface above the mean line a distance x away from the origin, and L is the overall length of the profile under examination